CHEMICAL VAPOR DEPOSITION OF GRAPHENE ON A DIELECTRIC SUBSTRATE AND ITS CHARACTERIZATION

Deepika Sharma
MSc Thesis
Master's in Photonics
University of Eastern Finland, Department of Physics and Mathematics
May 2012

TABLE OF CONTENTS

UNIVERSITY OF EASTERN FINLAND, Faculty of Science and Forestry
Master's in Photonics
Deepika Sharma: Chemical vapor deposition of graphene on a dielectric substrate and its characterization.
MSc thesis 50 Pages
Supervisor: Prof. Yuri Svirko, Tommi Kaplas
May, 2012

Keywords: Chemical vapor deposition, Graphene.

ABSTRACT

This thesis is focused on the synthesis and characterization of few layer graphene (FLG). Synthesis of FLG on a dielectric substrate was done using direct chemical vapor deposition technique (CVD). For direct deposition of graphene, quartz substrate with pre-deposited Cu film of 150nm thickness was used. In thermal CVD process, methane and hydrogen were used as process gases and methane was served as the carbon source. Annealing and cooling processes were done in hydrogen atmosphere. The transmittance of graphene samples in the visual and infra-red spectral range was measured using spectrophotometer and based on the observed results, number of graphene layers in the sample was calculated. Further characterization was done using Raman spectroscopy, scanning electron microscope (SEM) and atomic force microscopy (AFM).

Results show the presence of finger shaped regions of copper after thermal CVD process, where the formation of graphene is observed at copper-air interface and at copper-substrate interface. To remove graphene and copper film, oxygen plasma and $FeCl_3$ wet etching has been used respectively. Obtained finger like structures well corresponded to the result of ref [1], in which size of finger structures depend on the thickness of Cu thin film and the process temperature. SEM images and Raman spectra revealed the presence of graphene beneath finger like copper structures with the comparable quality as of graphene formed on the top of copper thin film. Based on observations it can be easily concluded that in the synthesis process of graphene, some carbon atoms penetrate through copper thin film and those that are near surface get accumulate on the surface and form graphene during cooling. Raman spectra helped to identify presence of bulk and few layers of graphene and Raman peaks demonstrate the existence of bulk graphite, FLG, mono and bi-layer graphene. Transmittance data gave

an approximate idea about the existence of two layers of graphene. Calculated number of layers from transmittance data is equal to ~1.42 where transmittance from graphene sample was ≈ 96.88%. Calculation of transmittance of graphene shows the dependency of transmittance on substrate.

In brief direct deposition of graphene using CVD can be considered as an effective way for synthesis of mono to few layers of high quality graphene on a dielectric substrate. Also the formation of finger like structures seems to reduce the effective number of graphene layers and as a result even after the presence of bulk graphite and few layers of graphene the transmittance is equivalent to ≈ 96.88% where transmittance of one layer of suspended graphene is ≅ 97.7%.

ACKNOWLEDGEMENT

I would like to express my sincere gratitude to Prof. Yuri Svirko and Tommi Kaplas, the thesis supervisors, for their sincere guidance, obliging suggestions and interesting and valuable ideas, which helped me a lot to carry out my project work in fruitful manner and to speed up the progress in this project.

I owe my thanks and affections to my parents and my friends, from whom I got mental support and affection every time in maintaining the work properly. At last I would like to thank the Department of Physics and Mathematics, University of Eastern Finland, Joensuu, for providing me the necessary facilities to carry out my work and also all the faculties, Department of Physics and Mathematics, University of Eastern Finland, Joensuu.

ABBREVIATIONS

AFM	Atomic Force Microscopy
CVD	Chemical Vapor Deposition
GNR	Graphene Nano-Ribbons
GO	Graphite Oxide
HOPG	Highly Ordered Pyrolytic Graphite
PECVD	Plasma Enhanced Chemical Vapor Deposition
PMMA	Poly Methyl Methacrylate
QHE	Quantum Hall effect
SEM	Scanning Electron Microscopy
SLG	Single Layer Graphene
UV-VIS-NIR	Ultraviolet-Visible-near Infrared

LIST OF FIGURES

LIST OF TABLES

CHAPTER 1

INTRODUCTION

Graphene is one of the groundbreaking discoveries of 21st century. After five decades of theoretical work on graphene it was first discovered by A. K. Geim and K. S. Novoselov in 2004 in Manchester University [2]. Similar to other carbon allotropes such as diamond, carbon nanotubes, and buckminsterfullerene, graphene is also famous for its unique electrical, optical and mechanical properties. Graphene is the first two-dimensional crystalline material, which consists of one-atom thick carbon layer. It is formed of sp^2-bonded carbon atoms packed in a honeycomb crystal lattice [2]. Each carbon atom has four valence electrons, which form three sp^2 orbitals and one p_z orbital. Three sp^2 orbitals form three in-plane covalent σ-bond which correspond to deep filled valence band while one p_z orbital form (bonding) π and (antibonding) π^*states perpendicular to the plane formed by σ-bonds. Both bonding and antibonding states form highest occupied valence band and lowest unoccupied conduction band respectively. In graphene both valence and conduction bands touch each other in Brillouin zone at K-point (center of the edge) as displayed in fig 1.1, where energy of electron is equal to Fermi energy (E_F). The point where valence and conduction band touch is called Dirac point and energy denoted by E_D. Dispersion curve of graphene is linear near low energy values which make effective mass of electrons and holes equal to zero.

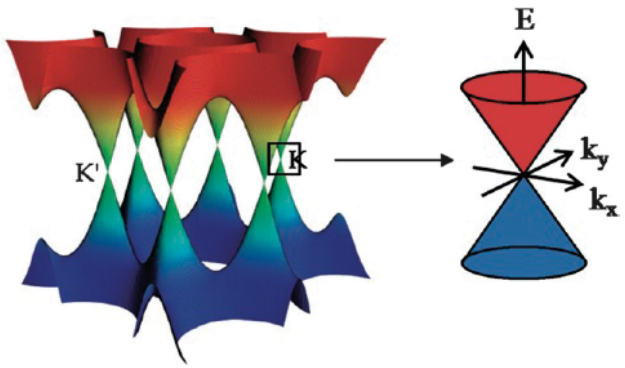

Fig1.1: Energy dispersion curve for graphene. Upper and lower surfaces show covalent and valence band respectively while k_x-axis and k_y-axis denote wave vector in x and y direction respectively. (C.N.R Rao at. el. [3]. Copyrights 2009 The Royal Society of Chemistry)

Due to zero effective mass of charge carriers near Dirac points they behave differently from the charge carriers in metal or semiconductor and can be described by two-dimensional Dirac rather than Schrödinger equation due to zero-band gap intrinsic graphene behaves as semi-metal. In addition, the presence of three in-plane σ-bonds causes hexagonal packing of carbon atoms in graphene, where each atom is covalently bonded with three adjacent carbon atoms and one electron left free from p_z orbital which allows graphene to conduct electricity.

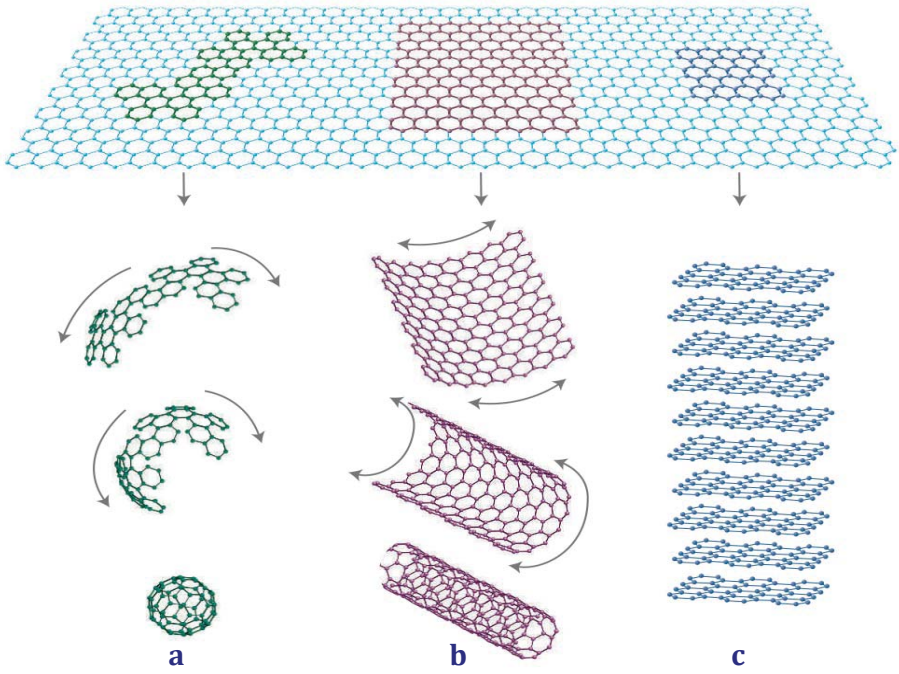

Figure 1.2: (a) Formation of Buckminsterfullerene (C_{60}) by single layer graphene: nanometer size rolled-up graphene (b) Formation of carbon nanotubes: rolled-up cylinders of graphene. (c) Formation of graphite: stack of graphene layers (Geim A.K. et. al [2]. Copyrights 2007 Nature publishing group).

Graphene is widely recognized as generic nanocarbon material, i.e it can be seen as a building unit of a number of carbon allotropes including carbon nanotubes, buckyball and graphite. For example, Fig. 1.2 shows that carbon nanotubes are made of rolled-up graphene and buckyballs are made of wrapped-up graphene [2,4]. In case of graphite, graphene layers are connected by relatively weak Van-der-Waals forces between adjacent layers. This enables obtaining graphene by graphite exfoliation.

Since the discovery of graphene, synthesis and characterization of graphene became prominent area of research. Graphene has attracted tremendous interest of scientists due to its unusual linear dispersion and presence of one free electron at every lattice site. These cause unique electrical, and optical properties including high current density, ballistic transport, high thermal conductivity, and optical transmittance. Similarly its strong in-plane covalent bonds give it unique mechanical and chemical properties along with super hydrophobicity at nanometer scale [5, 6].

There is a common belief that graphene has potential to revolutionize current technology from mini electronic chip to elevators in space. All these exceptional properties of graphene such as high room temperature carrier mobility i.e. up to ~ 27000 $cm^2V^{-1}s^{-1}$ [2, 7, 8, 9], high thermal conductivity exceeding ~3080 W/mK [10,11] and optical properties [12] favor the implementation of graphene in various devices. One aspect of recent research on graphene is the synthesis of high quality graphene for different industrial and research purposes.

There are many synthesis techniques for graphene like exfoliation of highly ordered pyrolytic graphite (HOPG), epitaxial growth on SiC, epitaxial growth on metal substrate, graphite oxide reduction, growth from metal-carbon melts, pyrolysis of sodium ethoxide, and chemical vapor deposition (CVD). Currently CVD is the most efficient – in term of the energy consumption and yield – technique for graphene synthesis. It enables in particular synthesis of graphene with large area and high quality, which is required for electronic and optoelectronic applications. However, CVD synthesis process enables graphene growth on metallic substrate therefore one needs to transfer synthesized graphene to dielectric substrate or other substrate. The transferring brings lack of scalability, inefficiency in electronic devices and large number of defects in the synthesized graphene samples. To avoid these unwanted effects of transferring Ismach et al. [13] has been recently demonstrate the direct deposition of graphene on dielectric substrate as shown in figure 1.3.

In direct deposition technique Ismach et al. [13] suggested to modify the conventional CVD process by replacing conventional copper foil with few hundred-nanometer thick copper film deposited on a dielectric substrate. The dewetting of copper films in CVD process resulted the formation finger like structures, while the dielectric substrate between these copper fingers was covered with high quality graphene. It was also shown that by increasing copper film thickness and reducing process temperature one can avoid dewetting of copper film in CVD

process and consequently can obtain continuous few layers of graphene. Figure 1.4 shows the dewetting of 450 nm and 100 nm Cu thin films at various CVD time [13].

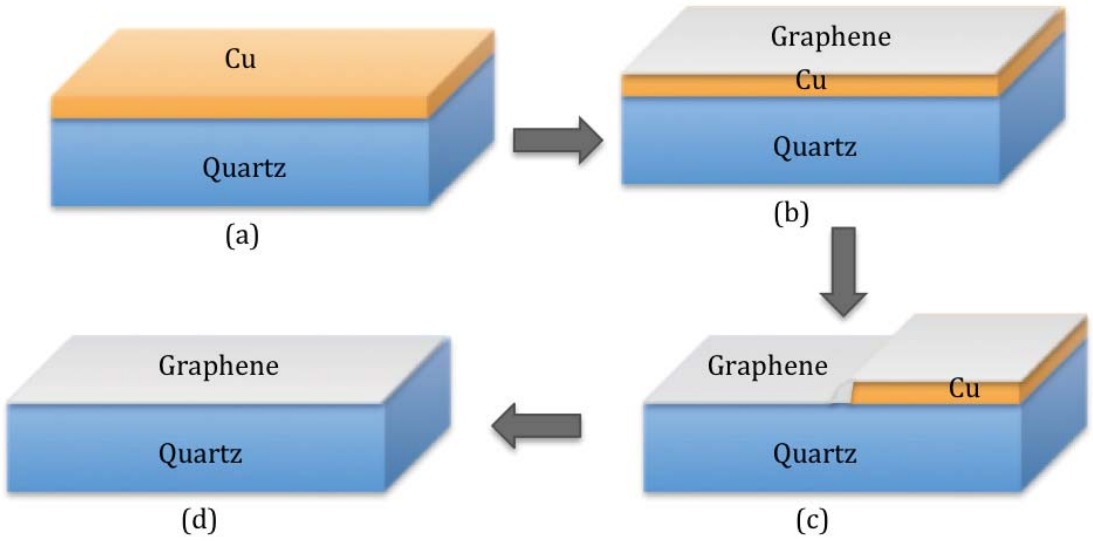

Figure 1.3: Schematic representation of direct deposition of graphene on dielectric substrate using CVD: (a) deposition of copper thin film by evaporation technique on dielectric substrate. (b) Graphene formation during Chemical vapor deposition. (c) Removal of copper from dielectric substrate due to metal dewetting and evaporation in CVD chamber. (d) Deposition of graphene on substrate after evaporation of metal.

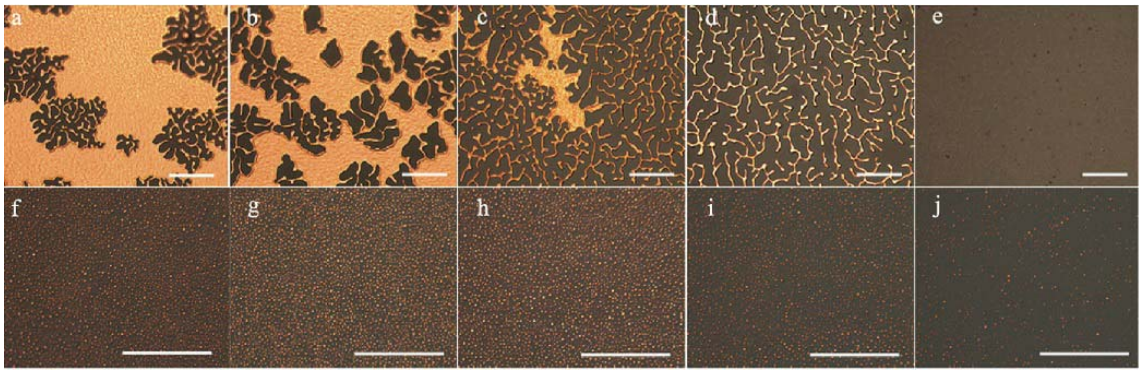

Figure 1.4: Dewetting and evaporation increment with CVD process time. (a-e) advancement of dewetting and evaporation for a 450 nm thick Cu film with the increment in CVD time for 15, 30, 60, 120 and 420 min, respectively. (f-j) Dewetting and evaporation for 100 nm thick Cu film at 15, 30, 60, 120, 300 min CVD time, respectively (Ismach A. et al. [13]. Copyright 2010 American Chemical Society).

Su Cy et al. [14] has recently demonstrate the growth of graphene on both copper-air and copper-substrate interface using pre-deposited ~300 nm thick copper film of quartz substrate in thermal CVD process. Very recently we performed [1] in depth study of catalytic growth of graphene on dielectric silica substrate by varying the thickness of copper thin film and temperature in CVD process. We showed that the quality of graphene grown on copper film is comparable to the graphene grown at the interface of copper and silica substrate. In this Thesis, we performed study of the physical-chemical processes responsible for the synthesis of graphene on silica substrate with pre-deposited copper thin film. Characterization of graphene, synthesized using ~150nm thick copper film on silica substrate, has been done using Raman spectroscopy, spectrophotometer, scanning electron microscopy, atomic force microscopy.

CHAPTER 2

ELECTRONIC AND OPTICAL PROPERTIES OF GRAPHENE

Graphene has extraordinary electronic and optical properties because of unusual bandstructure near the Fermi level. Since the band gap in few layer graphene (FLG) changes according to number of graphene layers and their stacking [15], in order to understand the properties of FLG one needs to understand its crystalline structure along with band-structure in the vicinity of the Dirac point.

Term “graphene” is conventionally used for a single layer of hexagonally packed carbon atoms. The graphene is a two dimensional hexagonal sheet of sp^2 hybridized carbon atoms [16] as shown in Fig. 1.2. Bi- and few layer graphene contain two layers and three to ten graphene sheets, respectively. There are three ways of stacking of single graphene layers. These are (i) hexagonal or AA stacking, (ii) Bernal or AB stacking and (iii) rhombohedral or ABC stacking as shown in Fig 2.1 [16, 17].

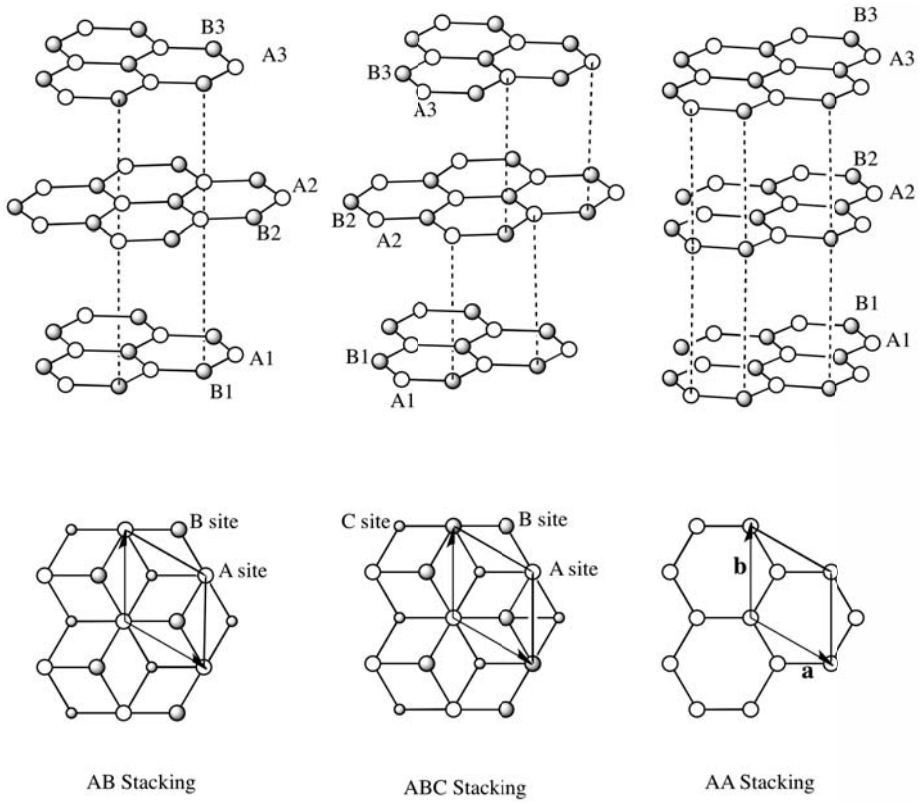

Figure 2.1: Most common structures and stacking sequences of graphene.

The interaction between layers results in the dependence of electronic properties of FLG on number of layers and stacking. Inter-layer interaction generates splitting in anti-symmetric π band of graphene, however it just slightly affect covalent band leaving covalent σ band remains intact. By increasing number of layers, ambipolar characteristics[1] of FLG diminishes due to very small overlap or no overlap between valence band and conduction band. However, in Bernal stacking family (ABAB..) three layer or higher layer graphene shows overlap of hole band and electron band large enough to enable ambipolar behavior of FLG. [15] Hence electronic properties of FLGs are strongly depends to its thickness [18] and the stacking of SLGs [15].

[1] Presence of both electrons and holes at Fermi level due to overlap between conduction band and valence band causes an effect in which charge carriers can be shifted from electrons to holes or vice-versa by changing polarity of applied gate voltage. This characteristic is known as ambipolar characteristic.

2.1 ELECTRONIC PROPERTIES:

Presence of one free electron at each lattice point in two dimensional crystal structure of graphene increases its conductivity and crystallinity, enabling electron to travel micron length path in material without any deflection. High electron mobility of graphene has been reported with maximum value of 15,000 $cm^2 V^{-1} s^{-1}$, where corresponding resistivity is 10^{-6} ohm-cm [7]. Along with graphene, graphene nano-ribbons (GNR) have also attracted a widespread attention because their electric properties vary depending on the configuration (see Fig. 2.1.1) due to change in the energy band diagram. For zigzag configuration GNR has metallic behavior, while for armchair configuration it may possess either metallic or semiconductor properties depending on the width of [2,19-21].

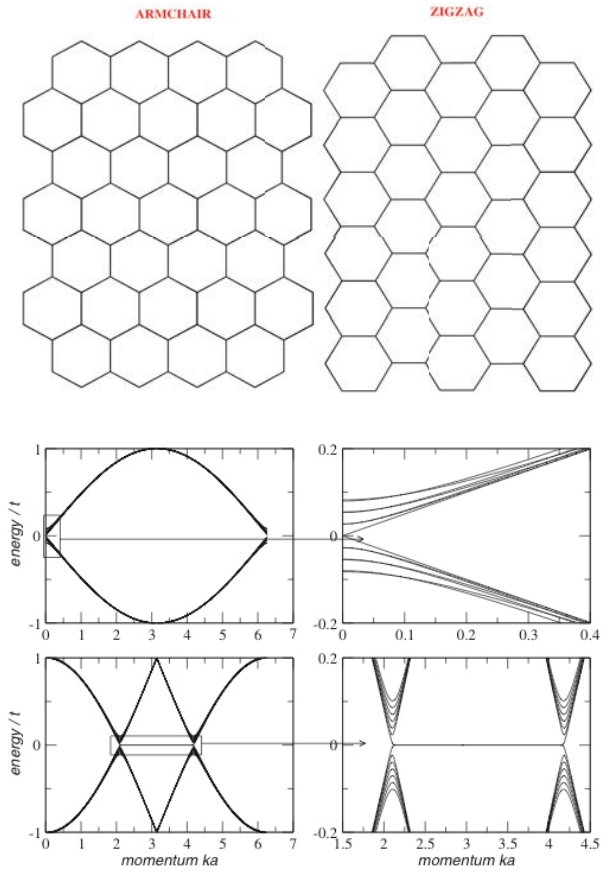

Figure 2.1.1 Top: Configuration of graphene nanoribbons. Bottom: Electronic dispersion curve for graphene nano-ribbons. (Left) Energy spectrum according to tight bonding equation for armchair (top) and zigzag (bottom) configured graphene nanoribbon with width N=200 unit cells. (Right) Zoom of the lower energy states shown in left side (Steve J. Koester [22]. Copyright 2009 Regents of the University of Minnesota).

Graphene has strong bonding, which makes it thermally stable material and causes less thermal noise. This stability gives rise to less signal to noise ratio and make it a prominent material for signal transmission and detection [23]. Hence, exceptional electric mobility and low Johnson noise[2] makes graphene the most desiring material for future electronic applications. [7].

Graphene is widely considered as replacement material for silicon in electronic industry. However, due to the presence of no energy gap in graphene there is no off stage in the transistor made of graphene and one can't replace silicon with intrinsic graphene in nanoelectronic devices. In order to solve this problem and to be able to manipulate electronic and optical properties of graphene one needs to modify Fermi level of graphene by doping i.e to convert it into n-type, p-type or hybrid doped graphene. There are different ways for doping in graphene such as using metallic substrate, which can alter the electronic structure, doping with nitrogen or boron atoms, adsorption of atoms or molecules at top or by introducing layer of different material underneath graphene grown on different substrate [24-29]. Doping with nitrogen converts graphene into n-type material while boron doping makes it p-type material. Intercalation of gold underneath graphene grown on ruthenium opens up energy gap, which is required for electronic, and optoelectronic applications [29].

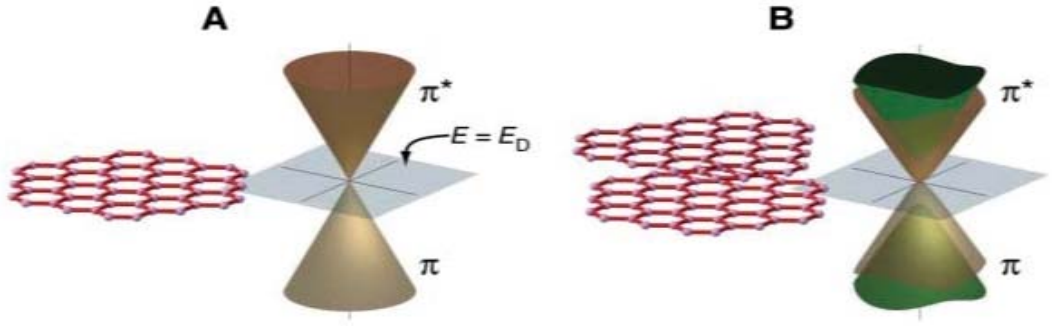

Figure 2.1.2: (a) Electronic structure of single layer graphene with conical shape and no energy gap. (b) Electronic structure of bi-layer graphene with parabolic shape and zero energy difference between two bands. The Dirac crossing points are at energy E_D. (Taisuke Ohta et al. 2006 [30]. Copyright American Association for the Advancement of Science.)

[2] Johnson noise is electronic noise, which is generated inside an electrical conductor at equilibrium due to thermal agitation of the charge carriers regardless of applied voltage.

Graphene is zero band gap material with semimetal behavior. It has conical electronic band structure in case of monolayer graphene as shown in Fig. 2.1.2 (a). The dispersion curve of graphene shows that in low energy region, energy of electron in graphene is directly proportional to momentum and results zero effective electron mass. As mentioned before the behavior of these relativistic electrons can be explained by (2+1) massless Dirac equations and these electrons called as Dirac fermions. Fermi velocity of these Dirac fermions is $\approx c/300$ where c is speed of light and therefore they behave as relativistic particles. Relativistic behavior of charge carriers in graphene leads new physical phenomena such as anomalous integer quantum hall effect. In general quantum Hall effect (QHE) in two-dimensional electronic system shows zero diagonal electric conductivity and quantized non-diagonal conductivity in strong magnetic field. The QHE is visible at high temperature only and quantization of non-diagonal conductivity is expressed as $\sigma_{xy} = -v\, e^2/h,$ where v is an integer or fraction. Based on the value of v it is called integer quantum Hall effect or fractional quantum hall effect. Unlike other two-dimensional electronic systems SLG shows integer quantum hall effect at room temperature. The Hall conductivity in case of graphene has an unconventional quantization as shown in Eq. 1, which is caused by the fact that the degeneracy of lowest Landau level (n=0) is twice smaller than higher Landau levels (n>0) and its energy is unaffected by magnetic field. In quantum mechanics, Landau levels are the discrete energy levels of cyclotron orbit of a charge particle in magnetic field. [23]

$$\sigma_{xy} = -\frac{e^2}{h}(2n+1), \qquad n = 0,1,2,3 \ldots \tag{1}$$

Here *n*= Landau level, *h* = Planck's constant and *e* = charge of electron. Landau quantization shows plateau corresponding to every integer in Hall conductivity diagram.

However, above expression for Hall conductivity is based on assumption of non-interacting Dirac quasiparticles. Graphene also demonstrates ambipolar characteristics at room temperature in gated transistor [7], which shows the ability to change the concentration of charge carriers or to switch charge carriers from electrons to holes and vice-versa by tuning gate voltage. Intrinsic graphene has slight overlap of valence and conduction band which causes the presence of both holes and electrons as charge carriers but applied gate voltage induces surface charge density on dielectric substrate which results into the shift of Fermi level and converts 2D- semimetal into complete hole or electron conductor [6,23].

Strong bonding between carbon atoms in graphene induces high electronic and thermal stability, which makes it promising material for gas detection. Also graphene is strictly two-dimensional material and provide larger surface area for gas detection. When gas molecule or atom attach to graphene surface it changes local carrier concentration one by one electron which causes step like changes in resistivity or conductivity. Gas detection by graphene can be maximized up to the detection of change of local concentration by one electron charge at room temperature. [31]

In case of bilayer graphene it has parabolic band structure as shown in fig 2.1.2 (b) and both conduction and valence band overlap at K and K' in Brillouin zone. Due to parabolic behavior of band near Dirac point, charge carriers don't have zero effective mass like in monolayer graphene. Hence, It has finite charge carriers, called massive Dirac fermion. Bi-layer graphene also shows anomalous Quantum Hall effect but unlike graphene, the Hall conductivity is $\sigma_{xy} = \left(\frac{e^2}{h}\right) n$, where $|n| \geq 1$. The zero level plateau corresponding to neutrality point n≈0, is missing and as a result it remains metallic at the neutrality points [32]. Similar to SLG few layer graphene also shows good gas adsorption property and high surface area [33]. Researchers showed that few layer graphene could easily be decorated with Pt, Ag and Au nano-particles, in a single step chemical process [3,34]. This decoration enhances its application in opto-electronics by increasing the bandgap of graphene. It has been determined that in case of epitaxially grown graphene on SiC substrate, it has ~ 0.26 eV band gap which decreases by increasing number of graphene layers and become zero at four graphene layers. Opening of band gap for monolayer graphene is caused by substrate-graphene interaction. Hence induced zero band gap in FLG causes structure to become metallic [35]. Furthermore, Zhang et al. has also demonstrated that graphene band gap can easily be modify at room temperature from 0 to 0.25 eV by tuning the voltage of a dual-gate bilayer graphene field-effect-transistor [36].

Both single- and few layer graphene have potential for electronics, memory, biotechnology, sensor, energy storage devices, opto-electronics etc. applications. Also, by modifying synthesis process one can easily improve the properties of synthesized graphene [17].

2.2 OPTICAL PROPERTIES:

Graphene is known for its impressive optical properties. Falkovsky et al. has demonstrated that optical conductivity of graphene depends on temperature, frequency and carrier concentration [37]. As mentioned before carrier concentration in graphene can be tuned by changing gate voltage, one can also change its optical reflectance and transmittance by changing gate voltage. Is has been shown that transmittance of graphene in visible range is constant and independent of frequency. Graphene transmittance in visible light is independent on the wavelength in a wide spectral range [38]. Specifically, opacity of monolayer graphene is equal to $\pi\alpha$ where α is the fine-structure constant [39], i.e. suspended monolayer graphene absorbs 2.3% of white light. This is the result of unusual low-energy electronic band structure of monolayer graphene. Similar to graphene, optical response of graphene ribbons can also be tuned in terahertz regime by applying magnetic field [40]. Recent results show that graphene/graphene oxide system *exhibits electrochromic behavior and enables tuning of both linear and ultrafast optical* properties [41].

Optical properties of thin films are commonly described in terms of dynamic or optical conductivity G= $\alpha c/4$ where c is the speed of light. In case of graphene the wavelength independent of G implies that the observable quantities like optical transmittance T and reflectance R are also universal. At normal incidence, $T \equiv (1 + 2\pi G/c)^{-2} = \left(1 + {}^{1}/_{2}\,\pi\alpha\right)^{-2}$ and $R \equiv {}^{1}/_{4}\,\pi^2\alpha^2 T$ [11]. The result is valid only if the collision rate of carriers (τ) is much smaller that the frequency and spatial distribution, $\tau^{-1} \ll \omega, kv$.

To analyze the optical properties of graphene in details lets consider optical (dynamic) conductivity σ as a function of temperature T, frequency ω, and chemical potential μ. General expression of optical conductivity of graphene can be obtained from reference [37]. Dynamic conductivity for higher frequencies $\omega \gg (kv, \tau^{-1})$ can be written as

$$\sigma(\omega) = \frac{e^2\omega}{i\pi\hbar}\left[\int_{-\infty}^{+\infty} d\varepsilon \frac{|\varepsilon|}{\omega^2}\frac{df_0(\varepsilon)}{d\varepsilon} - \int_{0}^{+\infty} d\varepsilon \frac{f_0(-\varepsilon) - f_0(\varepsilon)}{(\omega + i\delta)^2 - 4\varepsilon^2}\right], \qquad (1)$$

Here $f_0(\varepsilon) = \{\exp[(\varepsilon - \mu)/T + 1]\}^{-1}$ is the Fermi function where μ is the chemical potential, ε is energy and T is temperature in Kelvin.

First term in Eq. (1) refers to intra-band electron-photon scattering processes while the second term represents the direct inter-band electron transitions.

After integrating first term and replacing ω by $\omega + i\tau^{-1}$ to consider electron-disorder scattering processes we get the following expression for intraband conductivity, which is valid for $\mu \gg T$

$$\sigma^{intra}(\omega) = \frac{ie^2|\mu|}{\pi\hbar(\omega + i\tau^{-1})} \tag{2}$$

Where, μ can be found by measuring the carrier concentration $n_0 = (\mu/\hbar v)^2/\pi$.

Similarly the expression for inter-band conductivity can be obtained by integrating second term and considering infinitesimal quantity, $\delta \to 0$ to make the integral easy and evaluable at zero temperature. After simple mathematical calculation one gets

$$\sigma^{inter}(\omega) = \frac{e^2}{4\hbar}\left[G(\omega/2) - \frac{4\omega}{i\pi}\int_0^{+\infty} d\varepsilon \frac{G(\varepsilon) - G(\frac{\omega}{2})}{\omega^2 - 4\varepsilon^2}\right] \tag{3}$$

where,

$$G(\omega/2) = \begin{cases} \theta(\omega - 2\mu), & \mu \gg T, \\ \tanh \omega/4T, & \mu \ll T, \end{cases} \tag{4}$$

Here the principle value of integral with G($\omega/2$) is equal to zero and $\theta(\omega - 2\mu)$ is a step function which indicates the interband electron absorption condition at low temperature.

Now let us consider monolayer graphene at z=0 with dielectric constant $\epsilon_0 = \epsilon_g$, which is deposited on a substrate (z > 0) with $\epsilon_0 = \epsilon_s$, where ($\epsilon_s = 1$ for suspended graphene). The ac field is represented by the sum of incident and reflected waves in vacuum, z < 0, and by transmitted wave in the substrate. In the defined geometry, current in graphene can be given by

$$\boldsymbol{j}_x = \sigma(\omega)\delta(z)E_x\,. \tag{5}$$

Maxwell equation for graphene is

$$\nabla(\nabla.\mathbf{E}) - \nabla^2\mathbf{E} = \epsilon_0\frac{\omega^2}{c^2}\mathbf{E} + \frac{4\pi i\omega}{c^2}\mathbf{j} \tag{6}$$

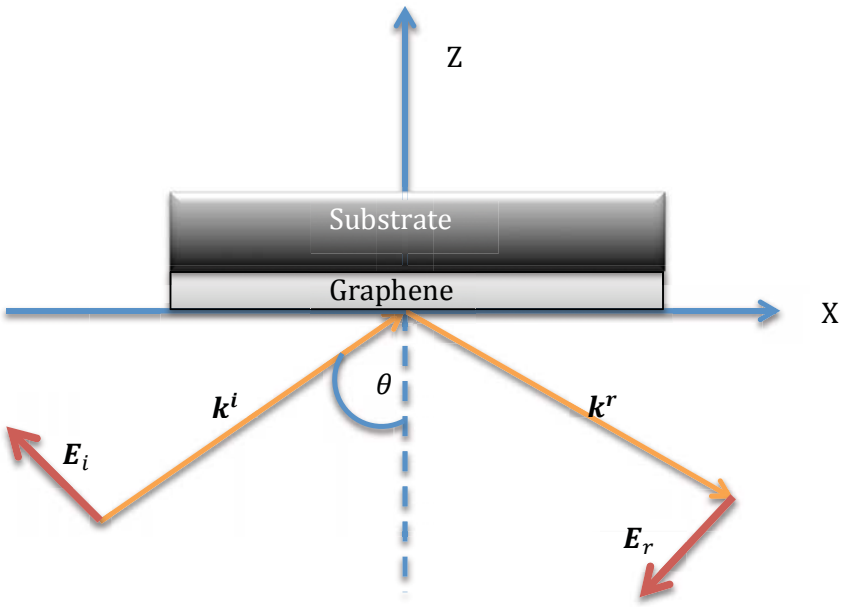

Figure 2.2.1: Schematic diagram of incident and reflected P-polarized light.

Here j is the conductivity current and ϵ_0 is an ion contribution in the dielectric constant. We are concentrating here on p-polarization, in which **E** lies in x-z plane and current j lies only along x-axis in layer.

By Fourier transforms of Eq. (9) w.r.t x coordinate, $\mathbf{E} \propto e^{ik_x x}$,

$$ik_x \frac{dE_z}{dz} - \frac{d^2E_x}{dz^2} - \epsilon_0 \frac{\omega^2}{c^2} E_x = \frac{4\pi i\omega}{c^2} j_x,$$

$$ik_x \frac{dE_x}{dz} + \left(k_x^2 - \epsilon_0 \frac{\omega^2}{c^2}\right) E_z = 0\,. \tag{7}$$

According to boundary conditions at z=0, the field component E_x must be continuous and the difference of electric-induction z component at the sides of monolayer:

$$\epsilon_s E_z|_{z=+0} - E_z|_{z=-0} = 4\pi \int_{-0}^{+0} \rho(\omega, k_x, z)\, dz \tag{8}$$

By replacing the expression of carrier density in Eq. 8 in terms of current from Eq. 5 and substituting E_z from the second Eq. (7) into (8)

$$\frac{\epsilon_s}{k_s^2}\frac{dE_x}{dz}\Big|_{z=+0} - \frac{1}{(k_z^i)^2}\frac{dE_x}{dz}\Big|_{z=-0} = \frac{4\pi\sigma(\omega)}{i\omega}E_x|_{z=0} \tag{9}$$

where

$$k_s = \sqrt{\epsilon_s(\omega/c)^2 - k_x^2}\,, \qquad k_z^i = \sqrt{(\omega/c)^2 - k_x^2}$$

After applying boundary conditions we find the amplitude for reflection (r) and transmission (t)

$$r = \frac{1-C}{1+C}\,, \qquad t = \frac{2}{1+C}\,, \tag{10}$$

$C = k_z^i[(4\pi\sigma(\omega)/\omega) + (\epsilon_s/k_s)]$. A result can be obtained for a graphene on dielectric substrate by replacing $\epsilon_s = n^2$, n is the refractive index of dielectric. At normal incident $\theta = 0$ hence $\sin\theta = 0$ and $\cos\theta = 1$.

$$k_z^i = \frac{\omega}{c}\cos\theta \quad \text{while } k_x = \frac{\omega}{c}\sin\theta$$

$$C = \frac{\omega}{c}\cos\theta\left[\frac{4\pi}{\omega}\frac{e^2}{4\hbar} + \frac{n^2}{\sqrt{\left(\frac{n\omega}{c}\right)^2 - \left(\frac{\omega\sin\theta}{c}\right)^2}}\right] \tag{11}$$

$$C = n + \frac{\pi e^2}{\hbar c} = n + \pi\alpha \approx n$$

Hence

$$t = \frac{2}{1+n} \text{ and } \mathrm{r} = \frac{1-n}{1+n} \tag{12}$$

Eq. 12 shows the dependency of transmittance and reflectance of graphene on refractive index of substrate, when it is deposited on a substrate. According to Eq. 12 opacity of graphene deposited on quartz substrate is ≈ 1.87 % at 550 nm.

In case of suspended graphene

$$\epsilon_s = 1 \text{ and } k_s = k_z^i$$

$$C = 1 + 4\pi\sigma(\omega)\cos\theta/c,$$

Reflected and transmitted amplitude under first order approximation of $\sigma(\omega)$

$$r = -2\pi\sigma(\omega)\cos\theta/c\,, \quad t = 1 - 2\pi\sigma(\omega)\cos\theta/c$$

Transmission coefficient for normal incident and for $T \ll \mu < \omega/2$,

$$|t|^2 = 1 - \frac{4\pi}{c} Re\sigma(\omega) = 1 - \pi \frac{e^2}{\hbar c}$$

Opacity of graphene on Quartz substrate at 550 nm wavelength is ≅ 2.2 [42], which is close to theoretical value. Hence the transmittance of graphene deposited on quartz is ≅ 97.8 %. As shown in figure 2.2.2, opacity of graphene layers is the linear function of number of graphene single layer with opacity of suspended SLG = 2.3%.

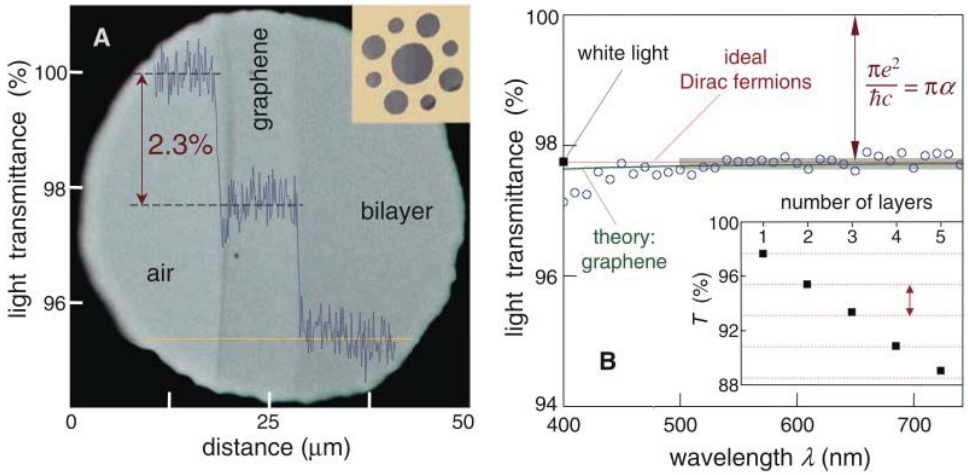

Figure 2.2.2 (A) Image of a 50-μm aperture which is partially covered by graphene and bilayer graphene. The scan profile shows the intensity of transmitted while light along the yellow light. (Inset) sample design: A 20-μm thick metal support with apertures of 20, 30 and 50-μm in diameter with graphene placed over them. (B) Transmittance spectrum of single layer graphene represented by open circles. Slightly lower transmittance for λ<500 nm is probably caused by hydrocarbon contamination [12]. Red line represents transmittance $T = (1 + 0.5\pi\alpha)^{-2}$ which is expected for two-dimensional Dirac fermions, whereas the green curve considers nonlinearity and triangular warping of graphene's electronic spectrum. Standard error of measurements is shown by gray area. (Inset) It shows the transmittance of white light as a function of number of graphene layers indicated by squares while the reduction in intensity by a factor $N * \pi\alpha$ is represented by dashed lines where N is the number of graphene layers (Nair R.R. et al [12]. Copyright 2008 Science Express.)

CHAPTER 3

TECHNIQUES FOR GRAPHENE SYNTHESIS

There are many techniques to synthesize graphene for different purposes. Based on the availability of facilities and quality of required graphene one can choose appropriate synthesis technique.

3.1 EXFOLIATION OF HIGHLY ORDERED PYROLYTIC GRAPHITE (HOPG)

Graphite is made of large number graphene layers attached with weak Van-der-Waals force. Exfoliation technique was the first method to obtain few layers of graphene from graphite by breaking interaction between neighboring graphene layers mechanically or chemically and peeling off graphene layers from graphite. First successful attempt to obtain few layers graphene by exfoliation was done by Novoselov et al. [7] and they also registered the production of single layer graphene using exfoliation. Novoselov et al. worked on a 1mm thick sheet of commercially available highly ordered pyrolytic graphite. On HOPG they formed few micron deep many mesas by dry etching in oxygen plasma. Obtained sample was put on photoresist and baked so that obtained mesas can stick to photoresist. Afterwards, layers were peeled off from graphite sheet using scotch tape and thin flakes, attached to photoresist were released in acetone and transferred to a Si substrate, which were found to be single to few layer graphene sheets. There have been many modulations to increase the efficiency of techniques. The main disadvantage of this process is its lower yield and throughput, and it is impractical for large-scale applications.

3.2 DESORPTION OF SI FROM SILICON CARBIDE (SIC)

Epitaxial growth of graphene by thermal desorption of Si from SiC is one of the most popular techniques. Graphene is grown by thermal decomposition of Si on (0001) surface plane of 4H-SiC or 6H-SiC substrate [43]. Number of graphene layers grown on substrate depends on the temperature and typical result is 1-3 graphene layers. Rollings et al. [44] was successful to produce one atom thick graphene film, which helped to attract the attention of semiconductor

industry. Further modifications were done using Ni thin film coated SiC substrate at lower temperature (750°C). This helped to obtain continuous large area graphene layers [45].

3.3 GROWTH FROM SOLID CARBON SOURCE

Graphene with large area and controllable thickness can be synthesized from solid carbon sources such as polymer films or small molecules deposited on a metal catalyst substrate at as low temperature as 800°C [46]. In studies the solid carbon source used was a spin-coated poly methyl methacrylate (PMMA) thin film (~100nm) and the metal catalyst substrate was a Cu film. A single uniform layer of graphene was formed on the substrate at a temperature as low as 800°C and as high as 1000°C for 10 min, with a reductive gas flow (H_2/Ar) at low temperature conditions [46].

3.4 REDUCTION OF GRAPHITE OXIDE

Basis idea of synthesis of graphene like sheets from graphite oxide is the exfoliation of graphene oxide into individual graphene oxide sheets and further chemical reduction of obtained individual graphene oxide sheets [47,48]. Graphite oxide (GO) can be achieved by oxidative treatment of graphite using any of three principal methods developed by Brodie [49], Hummer [50], and Staudenmeire [51]. The color of graphite oxide is lighter than that of graphite due to the loss of electronic conjugation brought about by oxidation and GO is hydrophilic in nature [52]. Graphite oxide is electrically insulating and because of that one cannot use it for electronic applications but it can be restored close to the level of graphite by chemical reduction of graphite oxide [53-56]. Due to hydrophilic nature of GO, after a suitable ultrasonic treatment it is easy to get graphene oxide thin sheets by exfoliation in water [47,57-59]. A detailed study of chemical reduction of exfoliated graphene oxide sheets with several reducing agents by S. Stankovich et al. [52] shows that hydrazine hydrate is the best to produce very thin graphene-like sheets.

3.5 GROWTH FROM METAL CARBON MELTS

Large area graphene can also be synthesized from carbon melts at low cost and high throughput. Amini et al. synthesized few layer to single layer graphene on metals from a molten phase [45]. The process involved the dissolution of carbon in molten metal at a

specific temperature and then nucleation of dissolved carbon and growth of graphene on the top of the melt at a lower temperature. To dissolve carbon in molten metal, metal is melted in contact with a carbon source such as graphite powder, or melted in graphite crucible. By keeping the metal melt in contact of carbon source at a certain temperature leads dissolution and saturation of carbon atoms in melt according to the binary phase diagram of metal-carbon. Decreasing the temp of carbon dissolved melt, solubility of carbon atoms decreases in melt and it gives rise the nucleation of excess carbon atoms on the surface which results as the growth of graphene on the surface of melt.

3.6 CHEMICAL VAPOR DEPOSITION

Few layers of graphene can be synthesized either by using thermal chemical vapor deposition (CVD) or plasma-enhanced chemical vapor deposition. In case of thermal CVD most of the graphene synthesis has been done using Ni or Cu substrate and precursor gas mixture of H_2 and CH_4 or other hydrocarbons and Ar gas as carrier gas. Quality and thickness of grown graphene depend on the cooling and heating rate, process temperature, ratio of gases, thickness and crystallinity of substrate. Yu et al. reported three to four graphene layers grown on polycrystalline Ni foils of 500 μm thickness, using thermal CVD method [60]. Similarly, X. Li et al. [61] has shown the successful growth of high quality, continuous graphene on Cu foil by thermal CVD. However, it was found that the growth of graphene on Cu substrate was self-limiting unlike Ni substrate, which is probably due to limiting Carbon solubility of Cu. The process with Cu substrate was claimed to be a surface-catalyzed process rather than a precipitation process, as has been reported for Ni [60].

Plasma enhanced chemical vapor deposition (PECVD) technique is also useful for graphene synthesis as this process reduces the consumption of energy and avoids the amorphous carbon formation [62-64]. Single to few layers of graphene using PECVD was first synthesized by J.J Wang et al. in [62, 63]. Graphene was synthesized on various substrates like Si, W, Mo, Zr, Ti, Hf, Nb, Ta, Cr, 304 stainless steel, SiO_2 and Al_2O_3, [62, 65] using radio frequency PECVD. By balancing the precursor gas ratio, temperature, substrate etc. one can further improve the yield of graphene.

The main disadvantage of CVD is that it uses gaseous raw material only, which makes it difficult to use this technology with other potential feedstocks. Also, in case of thermal CVD

there is always a need of transferring of graphene from metallic substrate to dielectric substrate and this step induces defects in the synthesized graphene. To avoid transferring, there is another method called direct deposition of graphene on dielectric substrate using CVD.

3.6.1 Direct chemical vapor deposition of graphene on a dielectric substrate:

Due to the disadvantages of previously known graphene synthesis techniques in terms of cost, quality of graphene, control on thickness and number of layers of graphene, large scale-fabrication and transferring step, there was a necessity of better, economic and effective method for large scale growth of high quality graphene with single or few layers. Hence, a method for direct CVD growth of single to few graphene layers on dielectric substrate is needed. Ismach et al. illustrated a method for direct chemical vapor deposition of single to few layer graphene film on dielectric substrate using a sacrificial copper film [64]. After performing direct CVD process on various substrates (single-crystal quartz, sapphire, silicon wafers with 300nm thermal SiO_2, and fused silica) with pre-deposited Cu film in the range of 100-450 nm, Ismach et al. demonstrated the formation of fingerlike structure due to dewetting of metal and illustrate that the areas in between the metal fingers vary in size and shape depending on the thickness of metal film and duration of CVD process. Significant results of direct deposition of graphene were obtained on quartz substrate and M-plane sapphire. It was also shown that the comparable results can be obtained on SiO_2 (300 nm)/silicon wafer and fused silica. In addition, It has been shown that in the case of thin metal film pre-deposited on substrate, metal films breaks into fingers or dots during temperature ramping-up before the CVD starts, and results in large uncovered area with graphene, hence in order to get continuous large area graphene one needs to use comparable thicker metal film [66].

CHAPTER 4

SYNTHESIS OF GRAPHENE

For direct chemical vapor deposition of few layer graphene on dielectric substrate we have used 2 inch diameter quartz substrate with 150nm thick thin film of copper on the top. Copper thin film deposition was done using thermal evaporation. Thickness measurement of Cu thin film was done using Veeco-dektak 150 and measured thickness was ≈150 nm. The setup used for CVD process has low ramping rate = 10°C/min. Prior to synthesis CVD chamber was cleaned by filling up N_2 gas at 110 mbar pressure in chamber and then pumping out the gas to make vacuum inside the chamber, the same process was followed twice with nitrogen gas and then with hydrogen gas. In annealing process heating was started at 100°C under 5.3 mbar pressure of H_2 (30ml, 30sccm) and continued till 700°C. At 700 °C H_2 gas was pumped out using vacuum pump and chamber was filled with process gases CH_4 and H_2. The ratio of process gases at 700 °C was 1:1 (H_2:CH_4) and initial pressure was 7.8 mbar with 15ml (30sccm) H_2 and 15ml (30sccm) CH_4. During graphitization process temperature raised from 700 to 950 and then after keeping the temperature at 950 °C for 1 min graphitization continued during cooling from 950 to 700 °C as shown in Fig. 4.3. Cooling of chamber started from 700 °C in H_2 (30ml) environment. After graphitization process gases pumped out and chamber was filled with H_2 (30 ml), which raised the pressure up to 7.5 mbar, to cool the chamber. Chamber cooling continued overnight.

Cooling and heating rate of the CVD system used was 10°C/min, i.e. it was lower than in conventional CVD systems. It causes in particular increase of the processing time. From the other hand, prolongation of the graphitization process enables the deposition of higher number of carbon atoms at the surface and increases the number of carbon atoms penetrated inside the copper thus resultant graphene grows on both copper-air and copper-silica interface. Schematic diagram of graphene formation beneath copper fingers is shown in figure 4.1. The dependence of quality and thickness of obtained graphene on thickness of Cu film and process temperature have been showed in [1]. The graphene synthesized beneath copper fingers preserved the shape of copper fingers. As shown in Fig. 1.3 formation of finger like structures and their size depends on thickness of copper thin film and process temperature. Raman spectra show that the quality of graphene grown at the surface and beneath Cu film

has comparable quality. Also, the obtained sample has finger like structures and Raman spectra has shown the presence of graphene in between fingerlike structures.

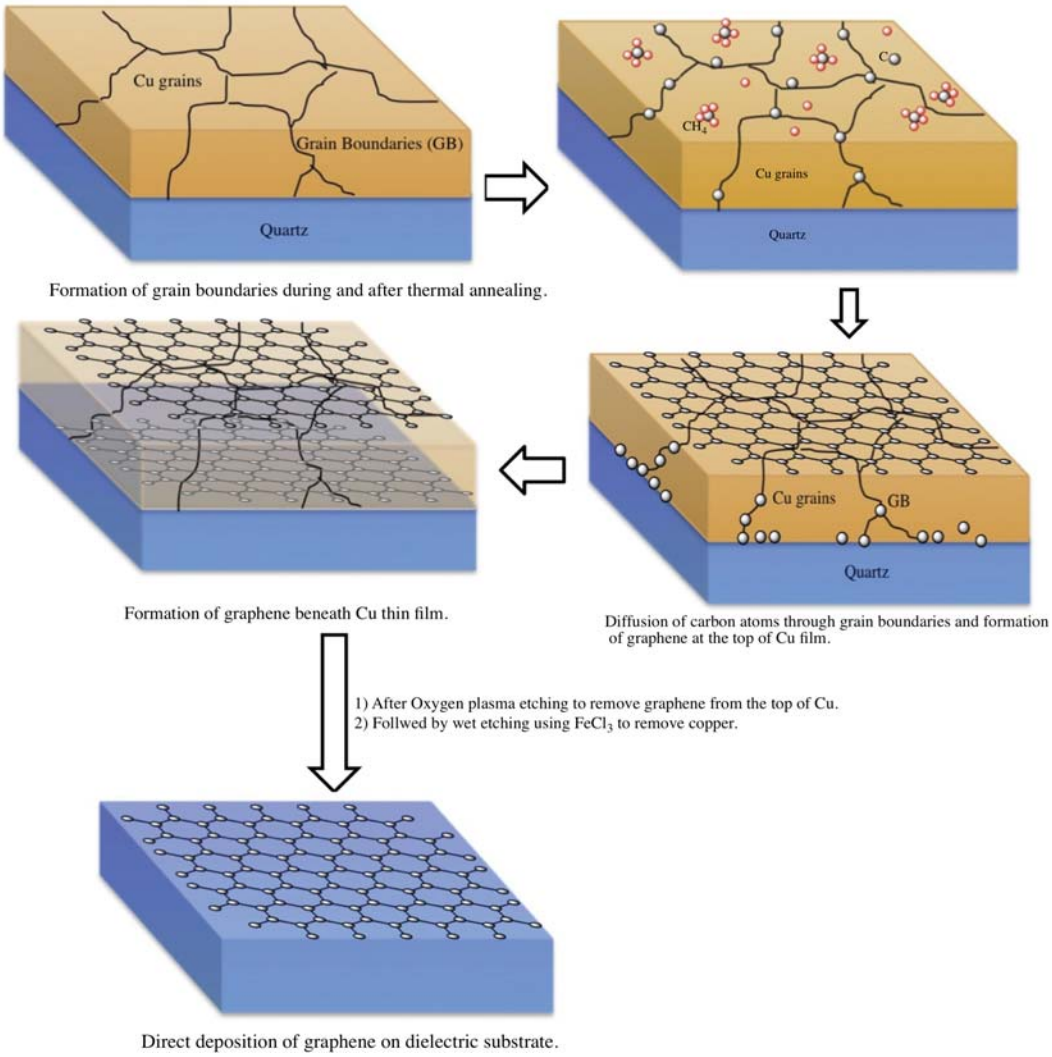

Figure 4.1: Schematic diagram of graphene growth directly on dielectric substrate. Step 1: Formation of Cu grain and grain boundaries during and after thermal annealing. Step 2: Dissociation of CH_4 precursors into carbon species and deposition of carbon atoms on Cu surface. Some of these carbon atoms diffuse through grain boundaries and reach on dielectric-copper interface. Step 3: Formation of graphene layer on the top of copper surface; meanwhile, the carbon atoms continue to diffuse through Cu grain boundaries (GB) and separate copper-substrate interface. Step 4: Graphitization of carbon atoms beneath copper layer leads to the formation of graphene in between copper-dielectric interface. Step 5: By removing copper thin film and graphene grown on copper film by wet etching, graphene directly deposited on dielectric can be obtained.

The CVD setup used for graphene synthesis is as shown in figure 4.2. It consist of vacuum pump directly attached to the chamber and fix glass tube for synthesis, which is covered with charcoal insulator for better insulation. This system provides an in-built programming option to change the ramping rate, dwelling time etc. to control the processes during synthesis. CVD chamber is connected to the pressure detector, which was used under 0.1 mbar resolution.

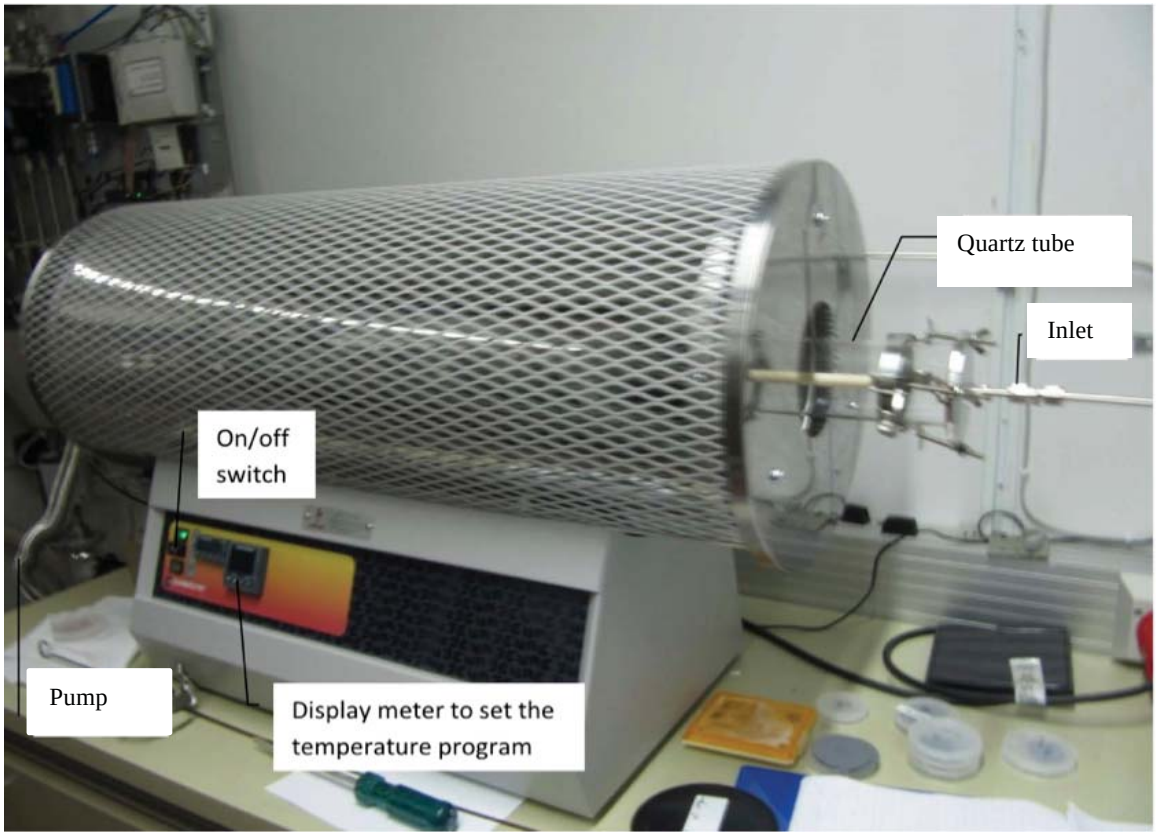

Figure 4.2: Chemical vapor deposition setup used for graphene synthesis. (Printed with permission of Department of Physics and Mathematics, University of Eastern Finland, Joensuu.)

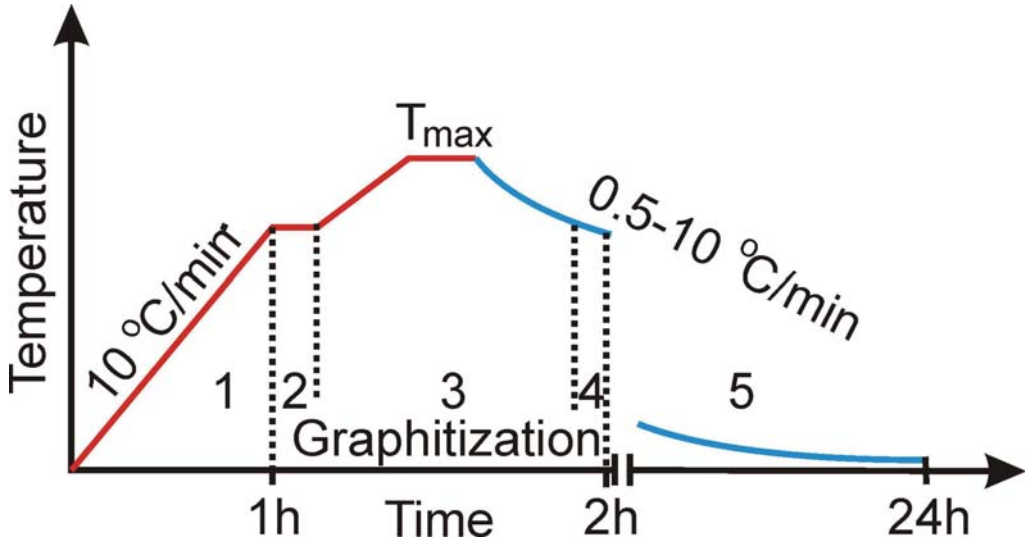

Figure 4.3: Schematic diagram of graphene synthesis process. Annealing from 100 to 700 °C with ramping 10°C/min. Graphitization from 700-950-700°C with ramping 10°C/min for first half and 2-10°C/min for second half, here T_{max} is 950°C. Cooling, which is almost exponential decrement and cooling continues overnight.

CHAPTER 5

CHARACTERIZATION OF GRAPHENE

Synthesis of graphene on Cu pre-deposited SiO_2 using direct deposition CVD technique resulted in the form of graphene on copper fingers and in between copper fingers. To characterize the observed sample we used following techniques:

5.1 SCANNING ELECTRON MICROSCOPY

To visualize the topography of synthesized graphene samples, they were studied using Scanning electron microscopy (SEM, LEO 1550 Gemini). To verify the graphene growth on copper-air and copper-quartz interface SEM images were taken after CVD graphene growth, shown in figure 5.1.1 (a, b, c), which shows the growth of graphene on the top of copper fingers. To verify the formation of graphene beneath copper fingers one needs to remove graphene from the top of copper film and from the dielectric substrate. It was done by etching samples in oxygen plasma. The obtained results are shown in Fig. 5.1.1 (d, e). $FeCl_3$ wet etching was further used to remove copper to obtain graphene beneath copper fingers (see Fig. 5.1.1 (f)).

SEM images confirmed the presence of graphene on the top, beneath and in between copper fingers. It also revealed the presence of tiny holes in copper finger and graphene grown beneath copper fingers. However the volumetric ratio of these tiny holes is much smaller than the area between fingerlike structures; hence the contribution of these tiny holes is insignificant. Photos taken using SEM shows that the fill factor is approximately 50%.

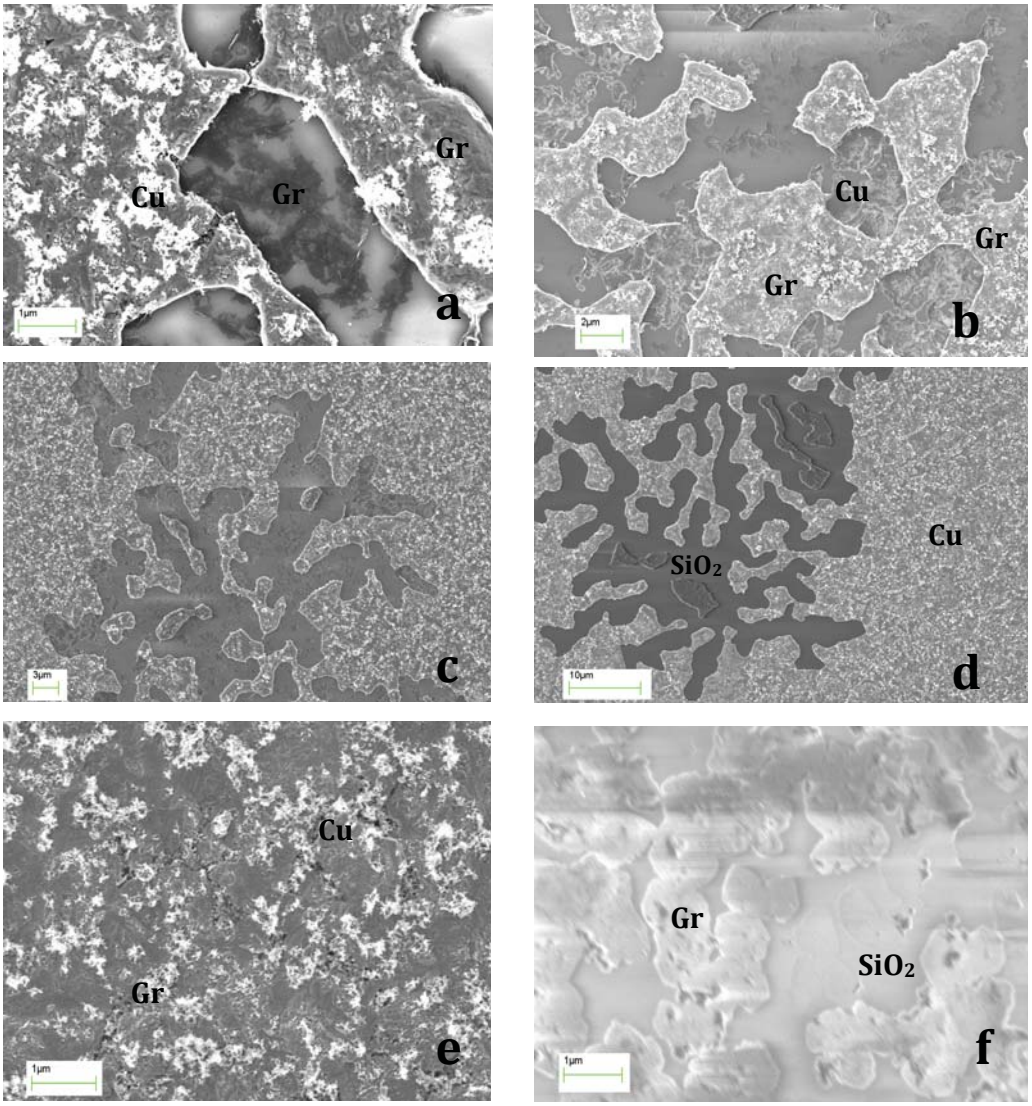

Figure 5.1.1 SEM images of 150nm thick Cu film deposited on SiO_2 substrate after CVD processing at 950-700°C (See fig. **a, b, c and e**), which show the formation of finger like structures after CVD process and presence of graphene beneath Cu fingers and above Cu fingers. Fig **e** also shows the presence of tiny holes in finger like structures and hence these holes result the formation of holes in graphene beneath Cu fingers. Fig **d** shows SEM image after oxygen plasma etching to remove graphite from Cu fingers and substrate. Fig **d** verifies the complete removal of graphene from substrate and from the top of copper film. Fig **f** shows the SEM image after removing Cu using $FeCl_3$. Fig **f** proves that copper finger structures preserves in the form of graphene fingers.

5.2 RAMAN SPECTRUM

Raman spectroscopy, which is based on the principle of inelastic or Raman scattering of monochromatic light, is an efficient technique to reveal the presence of various carbon allotropes. Interaction of monochromatic laser light with molecular vibrations, phonons or other excitations in the sample, result in the up and down shift of energy of scattered photons. This shift in energy provides information about the vibrational modes in the studied sample. Every material has its own vibrational modes hence by observing Raman spectra one can identify the material in the sample.

Analysis of Raman spectra is very useful to understand the quality of graphene sample and to estimate the number of layers in a graphene film by observing the intensity, shape and position of the G and 2D bands. In Raman spectra of graphene and other carbon materials with dominating sp^2 hybridization of atomic bonds, most intense features are the G peak at ~1580 cm^{-1} and 2D peak at ~ 2700 cm^{-1}, historically named G'. These two peaks are always observable in graphite samples [67]. G peak occurs due to the double degenerate zone center E_{2g} mode [68] while G' band or 2D peak is not related to G peak and appears due to second order of zone-boundary phonons. Zone-boundary phonons do not satisfy the Raman fundamental selection rule and because of that they do not appear in first order Raman spectra of defect-free graphite [69] but they give rise to a peak at ~1350 cm^{-1} in defected graphite, called D peak [68]. Both G and 2D Raman peaks vary in shape, position and relative intensity depending on the number of graphene layers [70].

Raman spectra were measured by Renishaw inVia Raman microscope using 5% laser power at wavelength of 514nm with beam size 2 μm. To verify the presence of graphene on copper fingers and in between fingers, Raman spectra were taken before oxygen plasma treatment and after oxygen plasma etching. Fig 5.2.1 shows that the ratio I(D)/I(G), which is often used as a measure of defect density of the graphite lattice [71,72] is in between 0.5 and 1. This indicates a high number of defects in graphene islands or the D peak is enhanced due to small size of flakes [71]. The ratio $I(G)/I(2D)$ can be employed to estimate the number of graphene layers [65]. In Fig. 5.2.1 I(G)/I(2D) is ~1.4 which shows the presence of 3-4 layers of graphene on copper fingers [65]. Fig 5.2.2 shows only copper peak, which reveals the absence of graphene on Cu surface after oxygen plasma etching.

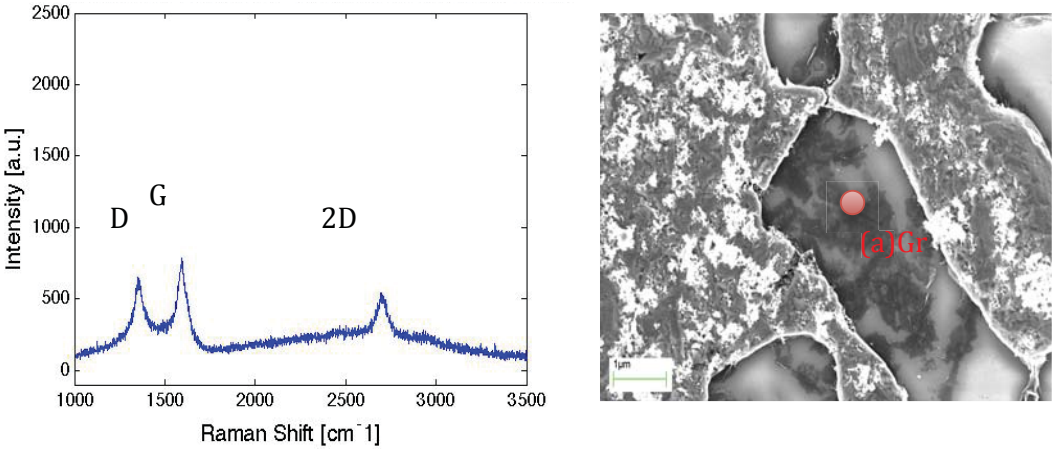

Figure 5.2.1: Raman spectra of graphene sample at point (a) before oxygen plasma etching.

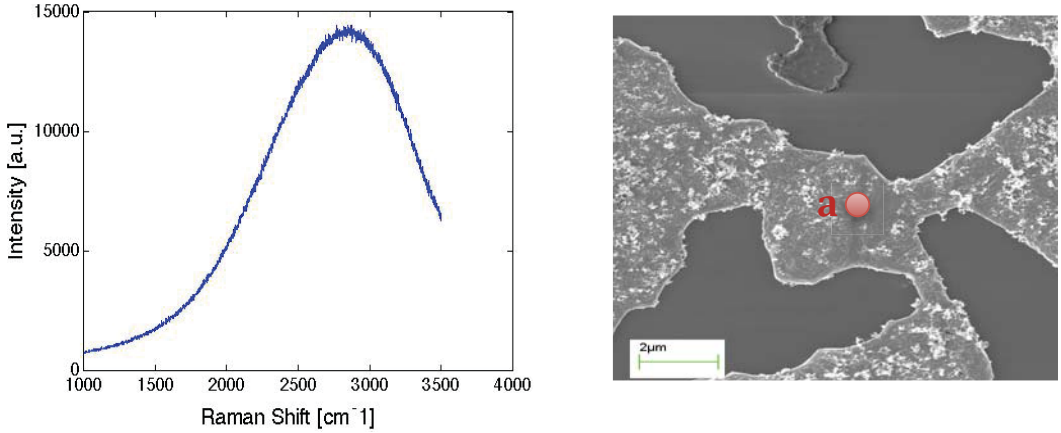

Figure 5.2.2: Raman spectra taken at point (a) after removing graphite by oxygen plasma etching.

Results show that oxygen plasma etching removes the graphene from the top of the copper fingers and SiO_2 substrate. After removing remains of copper with $FeCl_3$ wet etching we discovered the graphene beneath the copper fingers. Its crystallinity was comparable with that of graphene grown on the top and between Cu fingers. It is worth noting that graphene revealed beneath Cu fingers has the same shape as that of Cu fingers.

To examine the quality of graphene beneath copper fingers Raman spectra have been taken at various different locations (see Fig. 5.2.3) on graphene sample after wet etching.

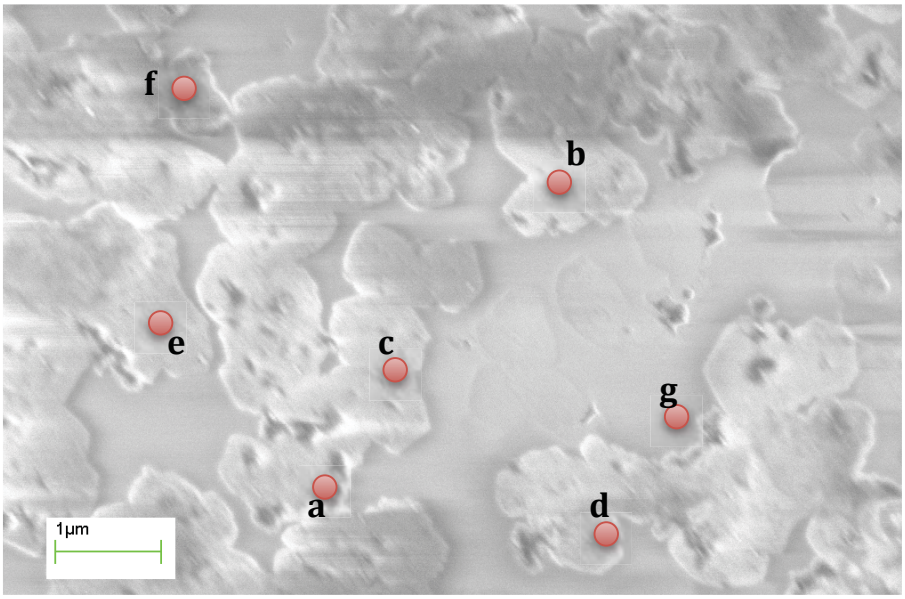

Fig 5.2.3: SEM image of graphene beneath Cu fingers after removal of Cu using $FeCl_3$ solution.

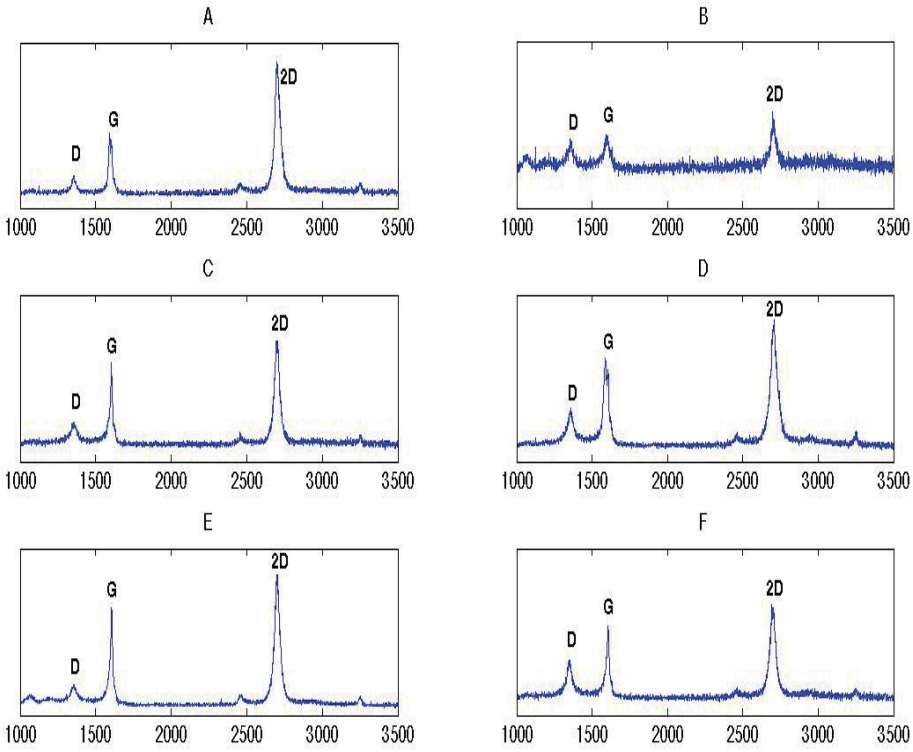

Figure 5.2.4: Raman spectra of finger shaped graphene area at corresponding points in figure 5.2.3.

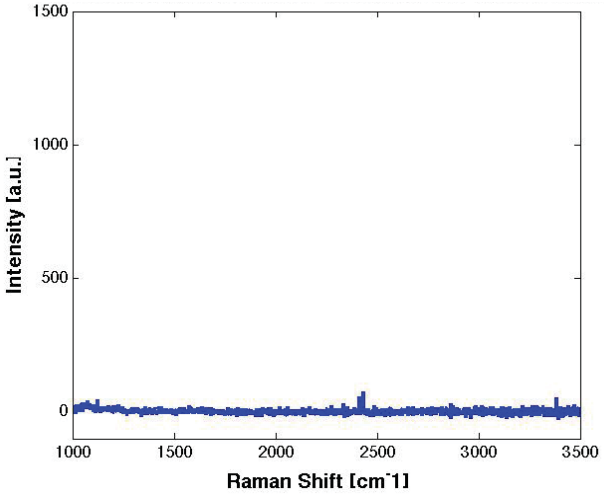

Figure 5.2.5 Raman spectra in between finger like structure at point (g) in figure 5.2.3.

Raman spectra in Fig. 5.2.4 indicate the presence of single and few layer graphene on the substrate after removing copper using $FeCl_3$ solution. While Fig. 5.2.5 shows that there was no graphene in between fingers formed during CVD process. G peak for bulk graphene appears at ~1594 cm^{-1}, while G peak of single layer graphene shifts from 1581 to 1604 cm^{-1} due to doping, which is quite normal for SLG after vacuum annealing and exposure to air [73,74]. In case of zigzag-edged graphene ribbons G-peak appears at ~1583 cm^{-1}[75].

In Figs. 5.2.4 (a, d), the G peak splits in two major peaks and there are small tips in both peaks, which show that the G peak is composed of multi peaks. A careful observation of G peaks in (a) tells that the two major peaks in splitting are at 1594 cm^{-1} and 1603 cm^{-1} (see Fig. 5.2.6) along with few minor peaks at 1597 cm^{-1} 1599 cm^{-1} and 1601 cm^{-1}. Similar major G peaks have been observed in ref [76] where peak at 1594cm^{-1} was observed for (bulk) graphene oxide nanosheet and peak at 1603cm^{-1} was observed for graphene nanosheet after reduction of graphene oxide by $NaBH_4$ where the reason of G peak at 1603cm^{-1} in case of graphene nanosheet was defects introduced by reduction procedure [76]. Based on this result one can assure the presence of bulk graphene and graphene with defects due to $FeCl_3$ wet etching process or by doping due to exposure to air. Similarly in (d) there are few minor splitting and two major splitting in G peak and the bandwidth is also relatively broad. Minor splitting peaks are at 1580 cm^{-1}, 1585 cm^{-1}, 1589 cm^{-1}, 1592 cm^{-1}, 1601 cm^{-1}, 1604 cm^{-1}, and 1607 cm^{-1} and major splitting peaks are 1589 cm^{-1}, and 1607 cm^{-1} (see Fig. 5.2.7). Peak at 1580 cm^{-1}, and 1585 cm^{-1}, show the presence of single layer to few layer

graphene. However relatively high intensity of 2D peak supports the presence of single layer graphene. It has already been examined that due to unintentional doping G peaks split and blue shifts for electron doping and red shifts for hole doping. Hole doping is considered due to oxygen or water molecule while electron doping can be caused by NH_3. Depending on electron density G peak splits for mono-layer graphene can range from 1590 to 1607 cm^{-1} for n-type doping [77]. Hence Peak at 1607 cm^{-1} is due to n-type of doping, which can be caused by nitrogen compounds.

It has been revealed that 2D peak in undoped bi layer graphene is the combination of 4 peaks known as $2D_{1A}$ $2D_{1B}$ $2D_{2A}$ $2D_{2B}$ while in three-layer graphene, it can be expressed by 6 Lorentzian peaks [78]. In case of single layer graphene 2D peak is sharp and nearly at 2700 cm^{-1}, but further increment in number of graphene layers leads broadening of 2D peaks and decrease in relative intensity. For three or more layers the intensity of $2D_1$ peaks decreases [70]. Hence Fig. 5.2.4 (a-f) show the presence of single layer to few layer graphene. All these peaks show the presence of single- to few layer graphene and the existence of doping with zigzag graphene edges. In Figs. 5.2.4 (a, c, d, e) a peak near ~2445 cm^{-1} is visible, called T+D peak, which is caused by $T+D_2$ combination, similar to the one observed in the carbon-implanted [79] and graphite crystal edge planes [80]

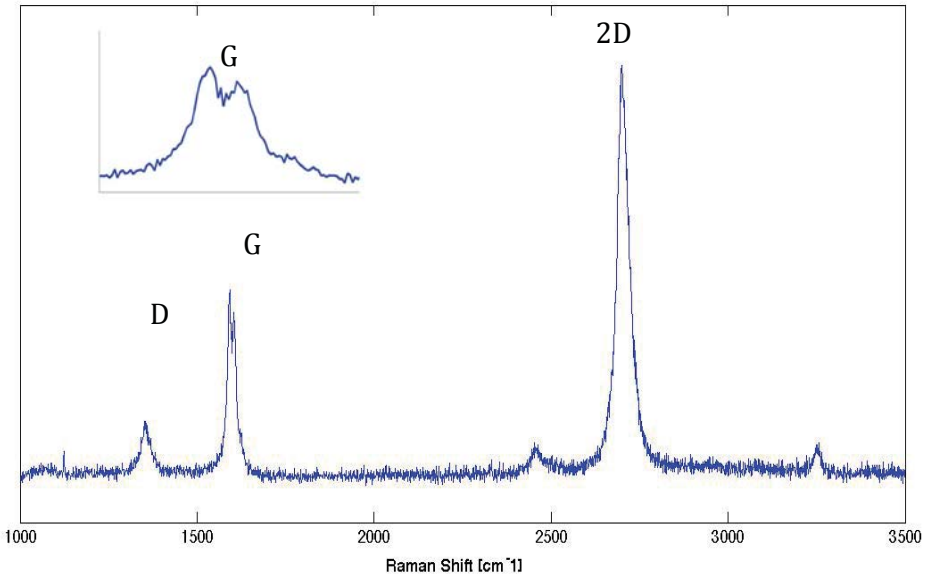

Figure 5.2.6: Raman spectra of graphene beneath Cu fingers with G peak splitting same as shown in fig. 5.2.4 (a).

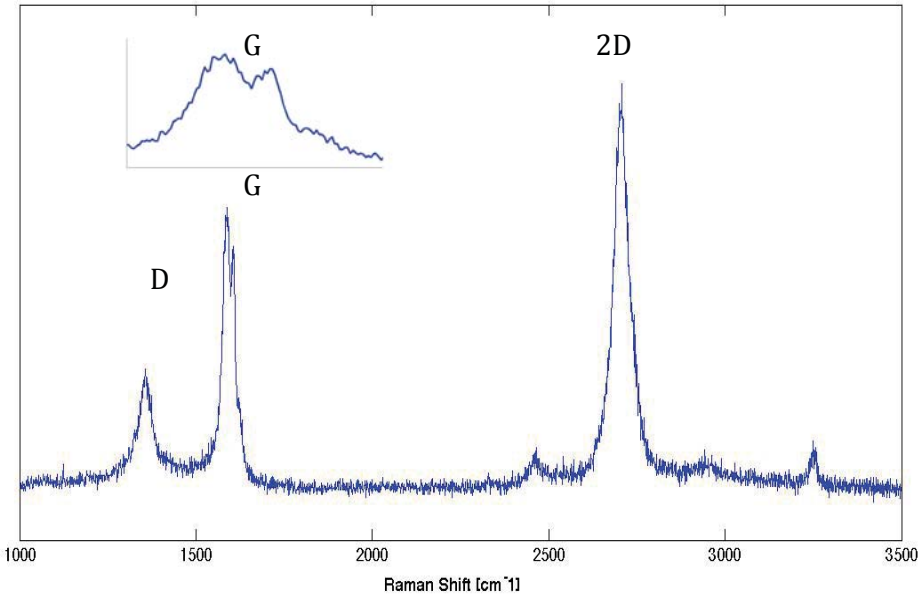

Figure 5.2.7: Raman spectra of graphene beneath Cu fingers with G peak splitting same as shown in fig. 5.2.4 (d).

Careful study of G and 2D peaks in Raman spectra assures the presence of mono- to few-layer graphene and bulk graphene with some doping due to exposure to atmosphere and wet etching process. It also shows the presence of zigzag-edged graphene.

5.3 OPTICAL CHARACTERIZATION

For optical characterization of synthesized graphene, transmittance of graphene sample was measured using Perkin-Elmer lambda UV/ VIS/ NIR spectrophotometer. Transparent quarts sample was used as reference. Transmittance was measured for sample with graphene on copper fingers, sample after removing graphite from the top of copper fingers and SiO_2 sample using oxygen plasma etching, sample with graphene sample only after removing copper using $FeCl_3$ solution.

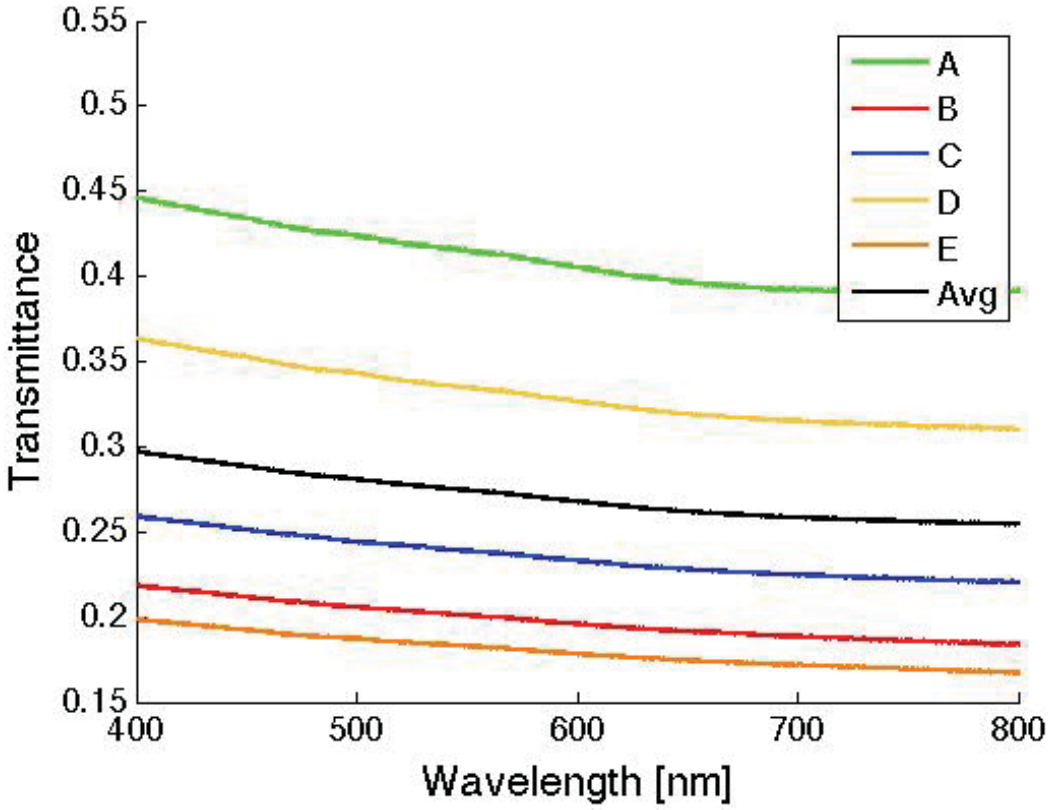

Figure 5.3.1: Transmittance spectra after removing graphite from copper fingers and substrate by oxygen plasma etching.

Table 5.3.1: Transmittance value at different points of sample after oxygen plasma etching, for 550 nm wavelength

Curve	Wavelength	Transmittance	Corresponding area covered by Cu
A	550 nm	0.4151	0.5849**A ***
B	550 nm	0.201	0.799**A***
C	550 nm	0.2387	0.7613**A***
D	550 nm	0.3345	0.7655**A***
E	550 nm	0.1829	0.8171**A***
Average	550 nm	0.2744	0.7256**A***

* **A** is the area of substrate.

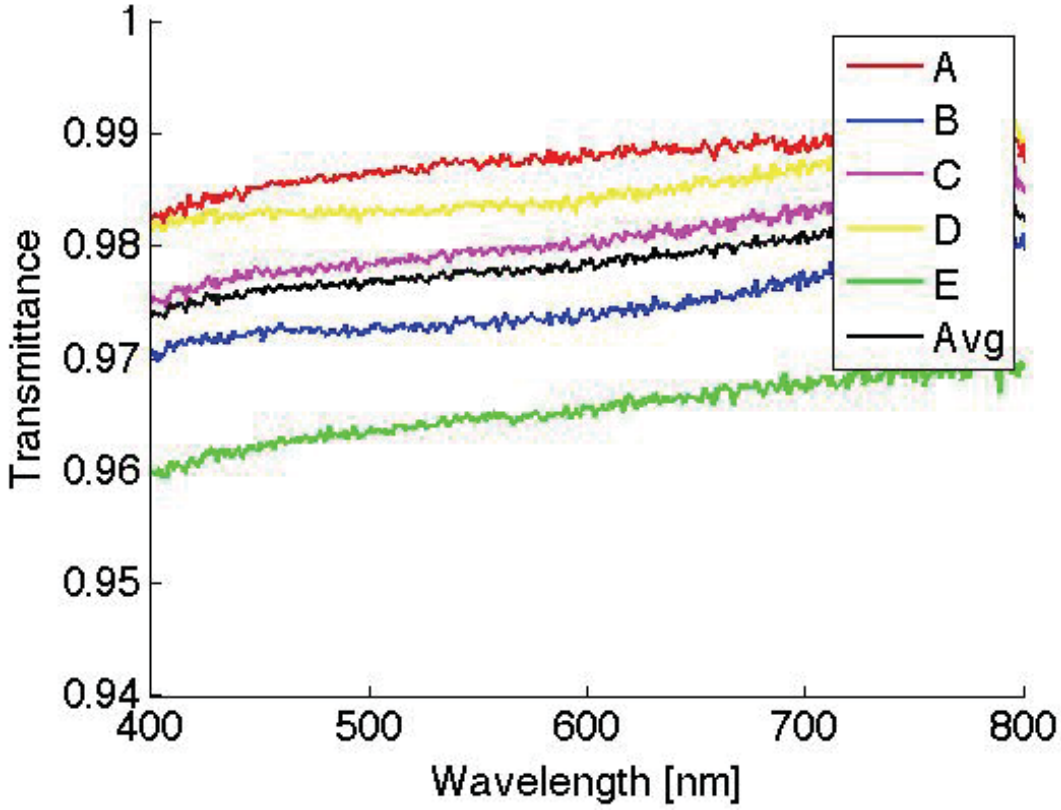

Figure 5.3.2: Transmittance spectra for graphene sample after oxygen plasma etching and $FeCl_3$ treatment.

Table 5.3.2: Various parameters calculated using transmittance spectra of sample before and after $FeCl_3$ treatment.

Name of parameters	Numerical Value
Wavelength	550 nm
Avg. Transmittance at 550 nm in fig 5.3.2	0.9774
Avg. Transmittance at 550 nm in fig 5.3.1	0.2744
Corresponding area of sample covered by Cu	0.7256**A***
Transmittance of graphene deposited beneath Cu fingers	0.9688
Corresponding number of graphene layers	=1.415≅ 2 layers

* **A** is the area of substrate.

To obtain the fraction of area covered with graphene, transmittance of graphene-copper-graphene sample was measured after removing top graphene layer from copper thin film and SiO_2 substrate. Transmittance from area covered with copper-graphene fingers is nearly zero

at 550nm while transmittance of silica substrate without copper-graphene fingers is 100% at 550nm. Average transmittance from copper-graphene substrate gives the fraction of area uncovered with copper-graphene fingers. Further transmittance measurement from graphene sample after removing copper thin film gives the sum of transmittance from area covered with graphene and area uncovered with graphene. Transmittance from graphene can easily obtain by using additive property of transmittance. As shown in Fig. 5.3.1 and Table 5.3.1 average value of transmittance from copper-graphene sample at 550nm is 0.2744. This value gives the fraction of area covered with copper-graphene fingers i.e. 0.7256*A, here A is the total area of sample. Transmittance from graphene is at 550nm is 0.9774 as shown in Fig. 5.3.2. By considering additive property of transmittance we can write

$$\left(\frac{0.2744 * A * 100 + 0.7256 * A * T}{A}\right) = 0.9774 \qquad (5.1)$$

Here transmittance through quartz substrate is 100%, and through graphene is *T*.

By solving Eq. 5.1 we get the 96.88% transmittance through graphene. Using 2.2% opacity of graphene on quartz at 550nm (taken from Ref. 42) effective number of graphene has been calculated. Result corresponds to 1.42-graphene layers that can be approximated with 2 graphene layers. To verify the result AFM was used to get the number of layers but graphene film was very thin and made it difficult to get AFM images hence no thickness data could be collected.

CHAPTER 6

RESULT AND DISCUSSION

In the present work, mono- to few layer graphene fingers has been directly deposited on dielectric substrate by incorporating direct chemical vapor deposition technique. Transmittance measurement of obtained graphene sample has shown 96.88% transmittance at 550 nm wavelength.

Direct CVD synthesis of graphene on a dielectric substrate has been achieved by using quartz substrate with pre-deposited 150nm thin copper layer and process temperature range $700℃ - 950℃ - 700℃$ with low ramping rate. Formation of Cu fingers was observed after thermal CVD process, with graphene on surface of Cu and beneath Cu fingers. By tuning thickness of copper thin film and process temperature, shape and size of Cu fingers can be controlled [13] and therefore the formation of graphene beneath Cu fingers. Growth of graphene beneath Cu fingers shows the penetration of carbon atoms through Cu film as shown in figure 4.1. Hence depending on the thickness of Cu film one can control the thickness of graphene beneath Cu fingers.

Previous experimental and theoretical data reveals that suspended monolayer graphene has 2.3% opacity, while the graphene deposited on dielectric substrate has opacity depending on the refractive index of substrate. Opacity of few layer graphene is directly proportional to the number of graphene layers, which helps to calculate the number of graphene layers in obtained sample directly from transmittance data. In this work, in order to identify the number of layers, we had to take into account both transmittances through sample with copper fingers and sample with graphene fingers. Transmittance measurement of sample before wet etching allows us to identify the area of sample covered by copper fingers, which can be used to calculate the transmittance of graphene. SEM images and transmittance data shows the formation of few layer (≈ 2 layers) graphene beneath Cu fingers.

Raman spectra of synthesized graphene sample show the shift in G and 2D peaks, which indicate the presence of doping due to annealing or air exposure [73,74]. Presence of G peak splitting in fig. 5.2.4 (a, c) indicates the presence of bulk graphite and graphene with zigzag

edges [75]. To avoid the formation of bulk graphite one can try to optimize the thickness of copper thin film and process temperature, pressure and ratio of process gases. Synthesis of high quality and large area few layer graphene by CVD can boost up the related research and technology to advance level.

One important thing, which comes into picture from combine result of Raman spectra and transmittance data, is that even the presence of impurities, doping or inhomogeneity in the sample does not reduce the transmittance drastically and effective transmittance is equivalent to 2 graphene layers. This result is of special importance for industrial applications because it indicates that it is possible to avoid the expensive and time-consuming processes necessary to synthesize and transfer single graphene sheets. The SEM images revealed that almost all finger like graphene islands are connected hence the created structure should not affect the conductance of sample.

Presence of graphene on both dielectric-air and dielectric-copper surface proves that due to low solubility of carbon atoms in copper, carbon atoms which are near the copper surface move upward during graphitization and form graphene while carbon atoms those are near the bottom of copper film form graphene beneath copper fingers and in between Cu fingers. It introduces a possibility that graphene formation beneath Cu fingers starts before the formation of copper fingers and continued till the end of graphitization process, because of the presence of graphene between copper fingers but at the level of Cu-substrate interface. Hence the obtained results also reveal the physics behind the formation of graphene beneath Cu layer and on the top of Cu fingers. Synthesis and optical measurements of graphene show the possibility of direct deposition of few layer graphene on dielectric substrate.

CHAPTER 7

CONCLUSION AND SUMMARY

In conclusion direct CVD method can be considered as an effective method for the synthesis of high quality mono- to few layer graphene on a dielectric substrate. SEM images and Raman spectra show the formation of graphene fingers on air-copper and copper-substrate interface with comparable quality. These graphene fingers retain the shape of copper fingers, obtained after CVD process. Shape and size of copper and graphene fingers can be controlled by tuning thickness of copper thin film, process temperature and annealing time. Raman spectra proved that oxygen plasma and wet etching by $FeCl_3$ are effective ways to remove graphene and copper film respectively.

From transmittance calculation it has been observed that the transmittance of graphene depends on dielectric constant of substrate and for suspended graphene transmittance is 97.7%. Also, opacity of few layer graphene is proportional to the number of graphene layers, where opacity of suspended graphene is 2.3%. Transmittance result shows that the formation of finger like structure seems to reduce the effective number of graphene layers and as a result irrespective of the presence of bulk graphite and few layer graphene effective number is ≈ 2 layers with transmittance $\cong 96\%$.

REFERENCE

[1] Kaplas T., Sharma D., Svirko Y. 2011. Few-layer graphene synthesis on a dielectric substrate. Carbon.

[2] Geim, A.K. and Novoselov, K.S. 2007. The rise of graphene. Nature Materials 6 (3): 183–191.

[3] Rao C.N.R., Biawas K., Subramanyam K.S., and GovindarajA. 2009. Graphene, the new nanocarbon. J. Mater. Chem., 19: 2457.

[4] Castro Neto A., Gulnea F. and Peres N.M.R. 2006. Drawing conclusions from graphene. Physics world.

[5] Chen J.H., Jang C., Xiao S., Ishigami M., and Fuhrer M.S. 2008. Intrinsic and extrinsic performance limits of graphene devices on SiO_2. Nature Nanotech, 3: 206.

[6] Geim A.K. and Kim P.2008. Carbon wonderland. Scientific American, 298: 90.

[7] Novoselov K.S., Geim A.K., Morozov S.V., Jiang D., Zhang Y., Dubonos S.V., Grigorieva I.V., and Firsov A.A. 2004. Electric field effect in atomically thin carbon films. Science, 306: 666-669.

[8] Zhang Y., Tan Y.W., Stormer H.L., and Kim P. 2005. Experimental Observation of. Quantum Hall Effect and Berry's Phase in Graphene. Nature 438:201.

[9] Berger C., Song Z., Li X., Wu X., Brown N., Naud C., Mayou D., Li T., Hass J., Marchenkov A.N., Conrad E.H., First P.N., and de Heer W.A. 2006. Electronic Confinement and Coherence in Patterned Epitaxial Graphene. Science 312:1191.

[10] BalandinA.A., Ghosh S., Bao W., Calizo I., Teweldebrhan D., Miao F., and Lau C.N. 2008.Superior Thermal Conductivity of Single-Layer Graphene. NanoLett8: 902.

[11] Ghosh S., Calizo I., Teweldebrhan D., Pokatilov E.P., Nika D.L., Balandin A.A., Bao W., Miao F., and Lau C.N. 2008.Extremely high thermal conductivity of graphene: Prospects for thermal management applications in nanoelectronic circuits. Applied Physics Letters 92:151911.

[12] Nair R.R. et al 2008. Fine structure constant defines visual transparency of graphene. Science 320 (5881): 1308.

[13] Ismach A., Druzgalski C., Penwell S., Schwartzberg A., Zheng M., Javey A., et al. 2010. Direct chemical vapor deposition of graphene on dielectric surfaces. Nano Lett 10 (5): 1542.

[14] Su C.Y., Lu A.Y., Wu C.Y., Li Y.T., Liu K.K., Zhang W. et al. 2011. Direct formation of wafer scale graphene thin layers on insulating substrates by chemical vapor deposition. Nano Lett11: 3612.

[15] Latil S., Henrard L. 2006. Charge Carriers in Few-Layers Graphene Films. Phys. Rev. Lett. 97: 036803.

[16] Hass J., de Heer W.A., and Conrad E.H. 2008. The growth and morphology of epitaxial multilayer graphene. J. Phys. Cond. Matter, 20: 323202.

[17] Choi W., Lahiri I., Seelaboyina R., and Kang Y. S. 2010. Synthesis of graphene and Its Applications: A Review. Critical Reviews in Solid State and Material Sciences 35.1: 52-71.

[18] ZhangY.et al.2009. Direct observation of widely tunable bandgap in bilayer graphene. Nature, 459: 820–823.

[19] Nakada K., Fujita M., Dresselhaus G. and Dresselhaus M.S. 1996. Edge state in graphene ribbons: Nanometer size effect and edge shape dependence. Phys. Rev. B54: 17954–17961.

[20] Brey L. and Fertig H.A. 2006. Electronic states of graphene nanoribbons. Phys. Rev. B 73:235411.

[21] Son Y.W, Cohen M.L. and Louie S.G. 2006. Energy gaps in graphene nanoribbons. Phys. Rev. Lett.97: 216803.
[22] Steve J. Koester, Ultra-smooth graphene nanoribbon formation using template nanoparticle crystallographic etching, University of Minnesota, Retrieved on 29 Jan 2012.
[23] Castro Neto A.H., Guinea F., Peres N.M.R. Novoselov K.S. and Geim A.K. 2009. The electronic properties of graphene. Rev Mod. Phys. 81: 109.
[24] Panchakarla, L.S. et al. 2009. Synthesis, structure, and properties of boron-and nitrogen - doped graphene. Adv. Mater. 21: 4726–4730.
[25] Wang X. et al. 2009. N-doping of graphene through electro thermal reactions with ammonia. Science, 324: 768–771.
[26] Wei D. et al. 2009. Synthesis of N-doped graphene by chemical vapor deposition and its electrical properties. Nano Lett. 9: 1752–1758.
[27] Ci L. et al. 2010. Atomic layer of hybridized boron nitride and graphene domains. Nature Mater. 9: 430–435.
[28] Rao C.N.R. et al. 2010. Some novel attributes of graphene. J. Phys. Chem. Lett.1: 572–580.
[29] Enderlein C., Kim Y.S., Bostwick A., Rotenberg E. and Horn K. 2010. The formation of an energy gap in graphene on ruthenium by controlling the interface, New J. Phys.12: 033014 1–9.
[30] Ohta T. et al. 2006. Controlling the Electronic structure of Bilayer Graphene. Science, 313: 951.
[31] Schedin F., Geim A.K., Morozov S.V., Hill E.W., Blake P., Katsnelson M.I., and Novoselov K.S. 2007. Detection of individual gas molecules adsorbed on graphene. Nature Materials, 6: 652.
[32] Novoselov K.S., McCann E., Morozov S.V., Fal′ko V.I., Katsnelson M.I., Zeitler U., Jiang D., et al. 2006. Unconventional quantum Hall effect and Berry's phase of 2π in bilayer graphene. Nature Physics, 2: 177.
[33] Ghosh A., Subramanyam K.S., Krishna K.S., Datta S., Govindaraj A., Pati S.K., and Rao C.N.R. 2008. Uptake of H2 and CO2 by graphene. J. Phys. Chem. C, 112: 15704.
[34] Muszynski R., Seger B., and Kamat P.V. 2008. Decorating graphene sheets with gold nanoparticles. J. Phys. Chem. C, 112: 5263.
[35] Morozov S.V., Novoselov K.S., Schedin F., Jiang D., Firsov A.A., and Geim A.K. 2005. Two-dimensional electron and hole gases at the surface of graphite. Phys. Rev. B, 72: 201401.
[36] Zhang Y. et al. 2009. Direct observation of a widely tunable bandgap in bilayer graphene. Nature 459 (7248): 820-823.
[37] Falkovsky L.A. and Varlamov A.A. 2007.Space-time dispersion of graphene conductivity. European Physical Journal B 56 (4): 281-284.
[38] Falkovsky L.A. 2008. Optical properties of graphene. J. Phys.: Conf. Ser. 129: 012004.
[39] Kuzmenko A.B., Van Heumen E., Carbone F., Van de Marel D. 2008. Universal infrared conductance of graphite. Physics Review Letter 100 (11): 117401.
[40] Liu J., Wright A.R., Zhang C., and Ma Z., 2008. Strong terahertz conductance of graphene nanoribbons under a magnetic field. Applied Physics Letter 93 (4): 041106-041110.
[41] Kurum U. et al. 2011. Electrochemically tunable ultrafast optical response of graphene oxide. Applied Physics Letter 98 (2): 141103.

[42] Ago H. et al. 2010. Epitaxial chemical vapor deposition growth of single-layer graphene over cobalt film crystallized on sapphire. American Chemical society, 4: 7407-7414.
[43] Wu Z., Ren W., Gao L., Liu B., Jiang C., and Cheng H. 2009. Synthesis of high-quality graphene with a pre-determined number of layers. Carbon, 47: 493.
[44] Rollings E., Gweon G.H., Zhou S. Y., Mun B. S., Mc Chesney J. L., Hussain B. S., Fedorov A.V., et al. 2006. Synthesis and characterization of atomically thin graphite films on a silicon carbide substrate. J. Phys. Chem. Solids, 67: 2172.
[45] Amini S., Garay J., Liu G., Balandin A.A., Abbaschian R. 2010. Growth of large-area graphene films from metal-carbon melts. J. Appl. Phys., 108: 094321.
[46] Sun Z., Yan Z., Yao J., Beitler E., Zhu Y., and Tour J. M. 2010. Growth of graphene from solid carbon sources. Nature letter, 468: 549-552.
[47] Stankovich S., Piner R.D., Nguyen S.T., Ruoff R.S. 2006. Synthesis and exfoliation of isocyanate-treated graphene oxide nanoplatelets. Carbon 2006; 44(15): 3342–7.
[48] Stankovich S., Dikin D.A., Dommett G.H.B., Kohlhaas K.M., Zimney E.J., Stach E.A., et al. 2006. Graphene-based composite materials. Nature, 442(7100):282–6.
[49] Brodie B.C. 1860. Sur le poidsatomique du graphite. Ann. Chim. Phys. 59:466–72.
[50] Hummers W., Offeman R. 1958. Preparation of graphitic oxide. J. Am. Chem. Soc. 80:1339.
[51] Staudenmaier L. 1898.Verfahrenzurdarstellung der graphitsaure. Ber. Dtsch. Chem. Ges. 31:1481–99.
[52] StankovichS. et al. 2007. Synthesis of graphene-based nanosheets via chemical reduction of exfoliated graphite oxide. Carbon 45: 1558-1565.
[53] Bourlinos A.B., Gournis D., Petridis D., Szabo T., Szeri A., Dekany I. 2003. Graphite oxide: Chemical reduction to graphite and surface modification with primary aliphatic amines and amino acids. Langmuir, 19(15): 6050–5.
[54] Hofmann U., Frenzel A. 1934. The reduction of graphite oxide by hydrogen sulfide. Kolloid-Z, 68:149–51.
[55] Xiao P., Xiao M., Liu P., Gong K. 2000. Direct synthesis of a polyaniline-intercalated graphite oxide nanocomposite. Carbon, 38(4): 626–8.
[56] Kotov N.A., Dekany I., Fendler J.H. 1996. Ultrathin graphite oxide- polyelectrolyte composites prepared by self-assembly. Transition between conductive and non-conductive states. Adv. Mater, 8(8): 637–41.
[57] Titelman G.I., Gelman V., Bron S., Khalfin R.L., Cohen Y., Bianco-Peled H. 2005. Characteristics and microstructure of aqueous colloidal dispersions of graphite oxide. Carbon, 43(3): 641–9.
[58] Szabo T., Tombacz E., Illes E., Dekany I. 2006. Enhanced acidity and pH-dependent surface charge characterization of successively oxidized graphite oxides. Carbon, 44(3): 537–45.
[59] Stankovich S., Piner R.D., Chen X., Wu N., Nguyen S.T., Ruoff R.S. 2006. Stable aqueous dispersions of graphitic nanoplatelets via the reduction of exfoliated graphite oxide in the presence of poly (sodium 4-styrenesulfonate). J. Mater. Chem., 16(2): 155–8.
[60] Yu Q., Lian J., SiriponglertS., Li H., Chen Y. P., and Pei S. S. 2008. Graphene segregated on Ni surfaces and transferred to insulators. Appl. Phys. Lett., 93: 113103.
[61] Li X., Cai W., An J., Kim S., Nah J., Yang D., Piner R., et al. 2009.Large-area synthesis of high quality and uniform graphene films on copper foils. Science, 324: 1312.

[62] Wang J. J., Zhu M. Y., Outlaw R. A., Zhao X., Manos D. M., Holloway B. C., Mammana V. P. 2004. Freestanding sub-nanometer graphite sheets. Applied Physics Letters, 85: 1265.
[63] Wang J., Zhu M., Outlaw R. A., Zhao X., Manos D. M., Holloway B. C. 2004. Synthesis of carbon nanosheets by inductively coupled radio‐frequency plasma enhanced chemical vapor deposition. Carbon, 42: 2867.
[64] Zhu M., Wang J., Holloway B. C., Outlaw R. A., Zhao X., Hou K., Shutthanandan V., Manos D. M. 2007. A mechanism for carbon nanosheet formation. Carbon, 45: 2229.
[65] Reina A., Jia X., Ho J., Nezich D., Son H., Bulovic V., Dresselhaus M. S., Kong J. 2008. Large Area, Few−Layer Graphene Films on Arbitrary Substrates by Chemical Vapor Deposition. Nano Letters 9: 30.
[66] Ismach A., Druzgalski C., Penwell S., Schwartberg A., Zheng M., Javey A., Bokor J., and Zhang Y. 2010. Direct Chemical Vapor Deposition of Graphene on Dielectric Surface. Nano Lett.,10:1542-1548.
[67] Vidano R.P. and Fischbach D.B. 1981. Observation of Raman band shifting with excitation wavelength for carbons and graphites. Solid State Commun. 39: 341-344.
[68] Tuinstra F. and Koenig J. L. 1970. Raman spectra of graphite. J. Chem. Phys. 53: 1126-1130.
[69] Nemanich R. J. and Solin S.A. 1979. First- and second- order Raman scattering from finite-size crystals of graphite. Phys. Rev. B 20: 392-401.
[70] Ferrari A.C. 2007. Raman spectroscopy of graphene and graphite: Disorder, electron-phonon coupling, doping and nonadiabatic effects. Solid State Communications 143: 47-57.
[71] Al-Jishi R., Dresselhaus G. 1982. Lattice-dynamical model for graphite. Phys. Rev B, 26(8): 4514–22.
[72] Chieu T.C., Dresselhaus M.S., Endo M. 1982. Raman studies of benzene-derived graphite fibers. Phys. Rev B, 26(10): 5867–77.
[73] Liu L., Ryu S.M., Tomasik M.R., Stolyarova E., Jung N., Hybertsen M.S., Steigerwald M.L., Brus L.E., Flynn G.W. 2008. Graphene Oxidation: Thickness-Dependent Etching and Strong Chemical Doping. Nano Lett., 8 (7): 1965-1970.
[74] Ni Z.H., Wang H.M., Luo Z.Q., Wang Y.Y., Yu T., Wu Y.H., Shen Z.X. 2010. The effect of vacuum annealing on graphene. J. Raman Spectroscopy, 41: 479-483.
[75] Yang R. et al. 2011. Observation of Raman G-peak split for graphene nanoribbons with hydrogen-terminated Zigzag Edges. Nano Lett., 11: 4083-4088.
[76] Feng M., Sun R., Zhan H., and Chen Y. 2009. Lossless synthesis of graphene nanosheets decorated with tiny cadmium sulfide quantum dots with excellent nonlinear optical properties. Nanotechnology 21 075601.
[77] Lin S.S., Chen B.G., Pan C.T., Hu S., Tian P., and Tong L.M. 2011. Unintentional doping induced splitting of G peak in bilayer graphene. Appl. Phys. Lett. 99: 233110.
[78] Malard L.M., Pimenta M.A., Dresselhaus G., and Dresselhaus M.S. 2009. Reman spectroscopy in graphene. Physics Reports 473: 51-87.
[79] Tan P.H., Deng Y.M., Zhao Q. 1998. Temperature-dependent Raman spectra and anomalous Raman phenomenon of high oriented pyrolytic graphite. Phys. Rev. B, 58: 5435–5439
[80] Tan P.H., Dimovski S., Gogotsi Y. 2004. Raman scattering of non-planar graphite: arched edges. Phil. Trans. R. Soc. Lond. A, 362: 2289–2310.